Remote Sensing of Environment 311 (2024) 114232

Contents lists available at ScienceDirect

Remote Sensing of Environment

journal homepage: www.elsevier.com/locate/rse

Estimation and validation of InSAR-derived surface displacements at temperate raised peatlands

Alexis Hrysiewicz [a,b,*], Jennifer Williamson [c], Chris D. Evans [c], A. Jonay Jovani-Sancho [c,d], Nathan Callaghan [c], Justin Lyons [e], Jake White [e], Joanna Kowalska [e], Nina Menichino [e], Eoghan P. Holohan [a,b]

[a] SFI Research Centre in Applied Geosciences (iCRAG), University College Dublin, Belfield, Dublin 4, Ireland
[b] UCD School of Earth Sciences, University College Dublin, Belfield, Dublin 4, Ireland
[c] UK Centre for Ecology & Hydrology, Bangor, United Kingdom
[d] School of Biosciences, University of Nottingham, Loughborough, United Kingdom
[e] Natural Resources Wales, United Kingdom

ARTICLE INFO

Editor: Zhe Zhu

Keywords:
Peatland
InSAR-derived peat surface displacements
In-situ peat surface displacements
Ground validation
Ecohydrology
Sentinel-1

ABSTRACT

Peatland surface motion derived from satellite-based Interferometry of Synthetic Aperture Radar (InSAR) is potentially a proxy for groundwater level variations and greenhouse gas emissions from peat soils. Ground validation of these motions at equivalent temporal resolution has proven problematic, either because of limitations of traditional surveying methods or because of limitations with past InSAR time-series approaches. Novel camera-based instrumentation has enabled in-situ measurement of peat surface from mid-2019 to mid-2022 at two large temperate raised bogs undergoing restoration – Cors Fochno and Cors Caron, in mid-Wales, United Kingdom. The cameras provided continuous measurements at sub-millimetre precision and sub-daily temporal resolution. From these data and Sentinel-1 acquisitions spanning mid-2015 to early-2023, we demonstrate that accurate peat surface motion can be derived by InSAR when a combination of interferometric networks with long and short temporal baselines is used. The InSAR time series data closely match the in-situ data at both bogs, and in particular recover well the annual peat surface oscillations of 10-40 mm. Pearson's values for the point-wise correlation of in-situ and InSAR displacements are 0.8–0.9, while 76% of differences are $< \pm 5$ mm and 93% are $< \pm 10$ mm. RMSE values between multi-annual in-situ and InSAR peat surface displacement rates are ~7 mm·yr^{-1} and decrease to ~3.5 mm for individual peat surface motion measurements. Larger differences mainly occur during drought periods. Multi-annual displacement velocities rates based on InSAR indicate long-term subsidence at Cors Caron (maximum −7 mm·yr^{-1}), while Cors Fochno exhibits subsidence at the centre and uplift at the margins (−9 mm·yr^{-1} to +5 mm·yr^{-1}). Because of the annual peat surface oscillations, however, more robust ground validation of the long-term peat surface motion rates derived from InSAR requires longer time-series of in-situ measurements than are presently available. Nonetheless, the InSAR-derived surface motion rates correlate well spatially with both peat dome elevation and peat thickness. In addition, the annual oscillations in surface motion are synchronous with or lag slightly behind groundwater level changes. A coarse ratio of 10:1 is observed between annual changes in groundwater level and peat surface displacement. Satellite-based InSAR derived from a fusion of short- and long-term temporal baseline networks can thus enable accurate monitoring of hydrologically driven surface motions of moderately degraded to intact temperate raised peatlands.

1. Introduction

Peat soils store an estimated 20–30% of global soil carbon (Drösler et al., 2008; Gorham, 1991; Köchy et al., 2015; Renou-Wilson et al., 2019; Yu et al., 2010). As a result of drainage for peat extraction, agriculture and plantation forestry, as well as fires, and other forms of habitat degradation, peatlands are estimated to contribute between 2% and 5% of global greenhouse gas (GHG) emissions (e.g., Joosten et al.,

* Corresponding author at: SFI Research Centre in Applied Geosciences (iCRAG), University College Dublin, Belfield, Dublin 4, Ireland.
E-mail address: alexis.hrysiewicz@ucd.ie (A. Hrysiewicz).

https://doi.org/10.1016/j.rse.2024.114232
Received 3 August 2023; Received in revised form 28 May 2024; Accepted 28 May 2024
Available online 4 July 2024

2016; Smith et al., 2014). The large uncertainty range reflects a lack of knowledge regarding both the extent of peatland modification and its impact on emissions. Reducing this knowledge gap has been become a priority in the current scientific research context and governmental policy guidelines. The ultimate goals are to protect peatlands and to restore their carbon sink capacity to partially mitigate global warming (Hiraishi et al., 2014; Leifeld and Menichetti, 2018; Letts et al., 2000). In addition, the preservation and restoration of peatlands are critical for conserving their unique flora and fauna, survival of which is intrinsically linked to the ecosystem's resilience to climate change (Renou-Wilson et al., 2019).

Traditionally, peatland monitoring has relied on in-situ measurements at local scale to estimate and to upscale various ecohydrological parameters: i.e., groundwater level changes, soil moisture changes, peat temperature and peat thickness. Extension of such monitoring of peatlands to regional, national, or global scales is a challenge. Indeed, approximately 3% of the world land area, amounting to 4.23 million km^2, is peat soil (Xu et al., 2018). This rises to 12% of the United Kingdom (UK) – c. 29,500 out of 241,930 km^2 (Evans et al., 2017; Smyth et al., 2017). Consequently, remote sensing methods over peatlands have been developed for: (1) vegetation and ecological mapping (e.g., Connolly and Holden, 2009; Connolly and Holden, 2017; Habib et al., 2024; Lees et al., 2018; Millard et al., 2020; Xu et al., 2018); (2) soil-moisture mapping (e.g., Balenzano et al., 2021; Balenzano et al., 2012; Millard and Richardson, 2018; Paloscia et al., 2013; Peng et al., 2021; Takada et al., 2009; Wagner et al., 2013; Xu et al., 2018); and (3) hydrological mapping (Asmuß et al., 2018; Bechtold et al., 2018; Kim et al., 2017) with large spatial coverage (regional and country scales) and relatively low cost. While much previous remote sensing work at peatlands mainly has concerned multispectral imagery, radar imagery is increasingly of interest (Minasny et al., 2019). A key advantage of radar remote sensing in temperate or humid climates is that observations are not hindered by cloud cover. Consequently, a consistent temporal resolution can be expected (e.g., up to 6/12-days with Sentinel-1 satellites).

Ground surface motion in peatlands has long been linked with ecological conditions, meteorological changes and/or hydrogeological variations (e.g., Bradley et al., 2022; Evans et al., 2021a; Hooijer et al., 2012; Howie and Hebda, 2018; Morton and Heinemeyer, 2019; Regan et al., 2019; Van den Akker et al., 2012). Long-term (i.e., multi-annual) subsidence has been connected with long-term lowering of the groundwater level. In addition, an annual rise and fall of the ground surface, termed "bog breathing" or "bog surface oscillation", has been observed on many peatlands and is linked with seasonal variation in precipitation and in groundwater levels (Howie and Hebda, 2018). Recently, empirical models have been proposed to relate in-situ subsidence measurements, groundwater level changes and carbon loss via GHG emissions (Hooijer et al., 2010; Hooijer et al., 2012; Hooijer et al., 2014). Obtaining representative in-situ measurements of peat surface motions is complicated, however, by the mechanical properties of peat and by the costs and/or limitations of traditional surveying techniques and equipment.

Most past efforts to measure peatland surface motions in-situ have focussed on the use of subsidence poles or precise levelling surveys (e.g., Howie and Hebda, 2018; Marshall et al., 2022). These survey methods offer the advantage of giving cm-scale to mm-scale precision, but have the disadvantages of being highly discontinuous in time (measurements typically monthly to yearly) and/or being cost-intensive in terms of equipment, fieldwork, and staff time. Other efforts have involved the installation of continuous Global Navigation Satellite System (cGNSS) stations (Reeve et al., 2013) or ultrasonic ground level sensors (Tampuu et al., 2023). These methods have the advantage of providing more continuous measurements in time (hourly to daily). However, cGNSS is relatively inaccurate to vertical motions that predominate at peatlands, such that the precision of measurement is on the order of several cm. In addition, secure installation and maintenance, over many years, of such expensive electronic equipment in a water-logged and highly acidic environment is challenging. Evans et al. (2021a) recently developed a low-cost, camera-based method to continuously monitor peat surface motion in-situ. The method involves a time lapse camera that can move vertically with the peat surface and that registers its motion with respect to a vertical pole fixed into the substrate below the peat. This high-precision (sub-millimetre), high-frequency (hourly) and low-cost method overcomes many limitations of previous techniques in term of accuracy, cost, and temporal sampling.

Satellite-based Interferometry of Synthetic Aperture Radar (InSAR) has made it possible to estimate ground surface motion at large scale, high to moderate spatial resolution, and, with open data, relatively low cost (for Sentinel-1 satellites). InSAR has been previously used to measure surface motion at peatlands in oceanic temperate (e.g., Alshammari et al., 2020; Alshammari et al., 2018; Fiaschi et al., 2019), continental temperate (Tampuu, 2022) and tropical climate zones (e.g., Hoyt et al., 2020; Zhou, 2013; Zhou et al., 2016). These past works used either C-band or L-band radar wavelengths and employed various InSAR time-series approaches: (1) Persistent Scatterers (e.g., Fiaschi et al., 2019); (2) Small-Baseline Subsets (SBAS) (e.g., Hoyt et al., 2020; Zhou et al., 2016); (3) Intermittent SBAS (Alshammari et al., 2018); or (4) Distributed Scatters (Tampuu et al., 2022). However, recent ground validation efforts show that existing approaches to InSAR computations on peatlands apparently fail to capture with accuracy both the longer-term trend of peat surface motion and the shorter-term variations in surface motion superimposed on that trend (e.g., Marshall et al., 2022; Tampuu et al., 2023). Consequently, improved application of InSAR to mapping peatland surface motion requires refinement of the processing techniques, but such refinement must go hand-in-hand with validation through an in-situ technique of compatible precision and temporal resolution.

In this study, we present an improved InSAR time-series approach for estimation of peatland ground surface motion based on combining the results of interferometric networks of differing temporal baselines. We test this approach at two semi-natural and partly modified temperate raised bogs, where ground validation of the InSAR results is possible against multi-annual time-series of in-situ surface motion derived at sufficiently high frequency and high precision from digital cameras. After presenting the two peatlands, we outline the refined InSAR time-series methodology, the in-situ instrumentation, and the statistical methods for ground validation. We then present maps and time series of the InSAR-derived peat surface motions as derived from networks of varying temporal baselines. We compare the InSAR-derived and the in-situ time-series of peat surface motion visually and statistically to highlight the significance of using the combined temporal baseline network approach. Finally, we show that the InSAR-derived peat surface motions are related to changes in groundwater level and variations in peat thickness at the two raised bogs. As for all InSAR approaches used to date, the refined method requires future work to test its accuracy on the wider variety of peat soil and landcover types. Nonetheless, our work should provide a basis for greater confidence in the future use of InSAR-derived estimates of surface motion for peatland monitoring and management.

2. Study sites

2.1. Ecological context and management history

Raised bogs in the UK, like in much of Europe, have been heavily modified and in some cases destroyed by human activities. Cors Fochno and Cors Caron are the largest remaining raised bogs in mid-Wales (UK) (Fig. 1). Cors Fochno, near the village of *Borth* (Lat: 52.49, Lon: −4.05), is located <1 km from the coast at elevations of <10 m.a.s.l. (see Fig. 1). Cors Caron, near the village of *Tregaron* (Lat: 52.22; Lon: −3.93), lies about 17 km inland at elevations of ~160–170 m.a.s.l.. Cors Fochno comprises one dome-shaped raised peatland area (see Fig. 1 and Fig. 2a). Cors Caron is divided into three dome-shaped raised peatland areas

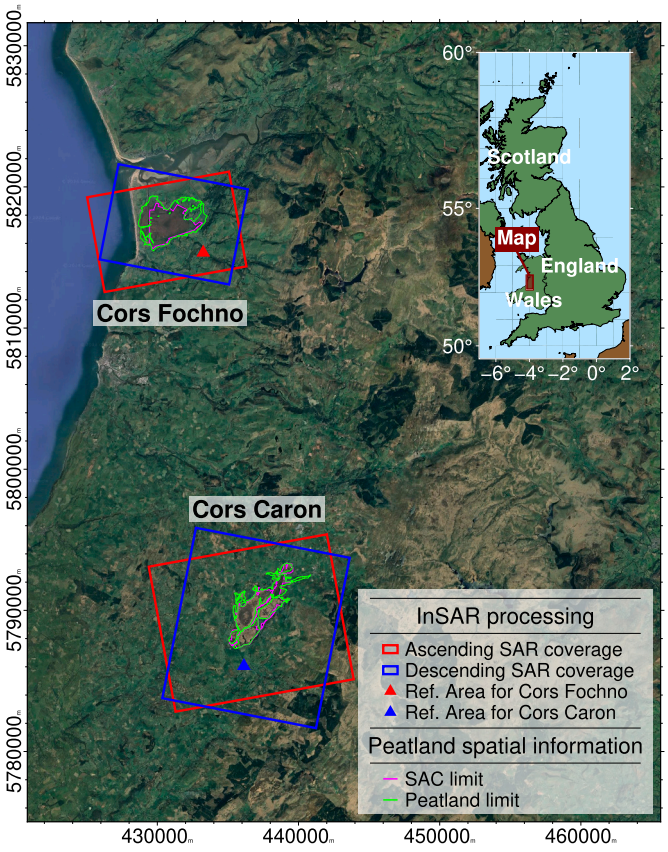

Fig. 1. Natural colour satellite image, from Google Earth (September 2019), with locations of the studied peatlands, the SAR data coverage (after cropping of Sentinel-1 images). The inset map shows the study area location within Great Britain. The grids are given in UTM Zone 30 N meters. Basemap Data: Google, Landsat / Copernicus / ©2023 TerraMetrics / ©2023 Airbus / ©2023 Maxar Technologies / IBCAO. Peatland-limit data: see Data availability section. Coastline from Global Self-consistent Hierarchical High-resolution Geography (GSHHG) database.

separated by a small river (*Afon Teifi*) and one of its tributary streams (see Fig. 1 and Fig. 2b). Although both study sites escaped destruction, they have been affected by historic land-use changes including drainage of the bog periphery for agriculture and peat cutting. The remaining areas of Cors Fochno and Cors Caron are designated as Special Areas of Conservation (SAC) (site codes: UK0014791 and UK0014790), the perimeters of which encompass 652 ha and 862 ha, respectively (see Fig. 2c and Fig. 2d). Internationally, both were NATURA 2000 sites (depreciated) and are currently sites for the EU LIFE programme, while Cors Fochno is in the Dyfi UNESCO Biosphere area.

The stratigraphic record at each site shows the infilling of a waterlogged topographic depression by decayed (i.e., humified) plant matter and the building of a gently sloped (< 5°) peat dome to heights of several metres above the surrounding land area. Borehole data show that the Cors Fochno peat lies directly on estuarine clay (Godwin, 1943), while the Cors Caron peat lies on lacustrine clay (Godwin and Mitchell, 1938). Peat thickness at each site increases from 1 to 2 m at the dome margins to 8–10 m at the dome centre. Overlying the basal clay at each site is a *phragmites* peat (reed dominated) layer, which at Cors Fochno is associated with a fen-wood peat layer (Godwin and Mitchell, 1938). There follows a well-humified *Sphagnum-Calluna* peat layer (moss-heather dominated), which is overlain by a poorly humified *Sphagnum* peat layer. Each of these *Sphagnum* peat layers is a few metres thick in the bog centre and thins toward the margin. Field inspections also indicate that the peat is generally less humified in the bog centre than at the bog edge, especially in the upper 10 cm. The classical fen to bog transition recorded in each successions reflects a shift from an ecology that was connected to alkaline groundwater or surface water sources (i.e., minerotrophic) to a present-day perched ecohydrological system that is highly acidic and is exclusively or predominantly rainfall-fed (i.e., ombrotrophic). The raised peat domes, as well as the rare flora and fauna they support, are therefore highly sensitive to climatic variations.

At both Cors Fochno and Cors Caron, the peat domes are mostly classed under the Terrestrial Phase 1 Habitat survey of Wales as unmodified raised bog (Fig. 2c and Fig. 2d). The vegetation cover here comprises a mix of mosses (*Sphagnum* sp.), heather (*Calluna vulgaris*), cross-leaved heath (*Erica tetralix*), bog myrtle (*Myrica gale*) and bog cotton sedge (*Eriophorum*). Marginal to the domes are areas classed as modified bog, where the dominant vegetation types are rushes (*Juncus* sp.) and purple moor grass (*Molinia caerulea*). Other marginal peat areas are classed as marginal swamps dominated by reeds (*Phragmites australis*). To the west and north of the Cors Caron western dome, there are additionally several areas classed as fen ("valley mire"), which are dominated by purple moor grass, hairgrass (*Deschampsia cespitosa*), sedges (*Carex*) and rushes. Small areas of oak (*Quercus)* and willow (*Salix* sp.) woodland occur along the southern and eastern borders of the Cors Fochno SAC, and a large area of willow scrubland mapped as underlain by peat soil lies to the northeast of the Cors Caron Western dome. Outside Cors Fochno SAC and within the Cors Fochno SAC, several areas mapped as underlain by peat soil are classed as marshy grassland or grassland.

In light of their ecological importance, both sites have been subject to extensive restoration works since their SAC designation in the 1980s. The majority of the periphery of the Cors Fochno SAC has an overdeepened drainage network of approximately 14 km. Internally, there are over 23 km of large to medium ditches within the SAC, many of which pass through the central "unmodified bog" area. Nearly all drains have been dammed as part of hydrological restoration works, mainly over the last 30 years. The period 2000–2016 saw extensive drain blocking, mainly on the south of the site and to a lesser degree on the eastern part of the dome. Between 2016 and 2022, a 55-km long network of contour bunds was constructed as part of the LIFE Welsh Raised Bog Project (see Fig. S1 in Supplementary Materials). Cors Caron has been subject to several restoration attempts via rewetting since the 1990s, when 300 large peat dams were built initially around the peripheries of all three bog domes (Schulz, 2004). In the 2000s, smaller dams were built within the peat cutaway areas up to the peat cliff, and observed surface cracks and ditches were blocked by using plastic piling. Since 2020, a 64-km long network of low-elevation contour bunds has been installed on the domes.

2.2. Climatological and meteorological context

The island of Great Britain falls within the oceanic temperate climate zone (Cfb) of the Koppen climate classification scheme. This is exemplified for the study period (2015–2022 inclusive) by data from two weather stations located on or beside Cors Fochno and by data interpolated from the regional stations of the UK Meteorological Office (Fig. 3). The climate varies little between Cors Fochno and Cors Caron, since the distance between them is about 30 km and the elevation change is <200 m. Winters are cool and summers are generally mild; temperatures rarely go below 0 °C or above 20 °C. Precipitation is frequent, and clouds are common. Seasonal oscillations in rainfall and temperature occur with well-delineated summer and winter periods. Average precipitation is 1100–1400 mm·yr^{-1} and average annual air temperatures are 6–7 °C.

Four relatively hot and dry summers occurred in Wales in 2018–2021 inclusive (Fig. 3). Summer 2018 had a particularly strong coincidence of high temperature and low rainfall that resulted in a several weeks long period of drought. Although not reaching the definitions of drought, a similar coincidence of high temperature and low rainfall occurred in summer 2021 also.

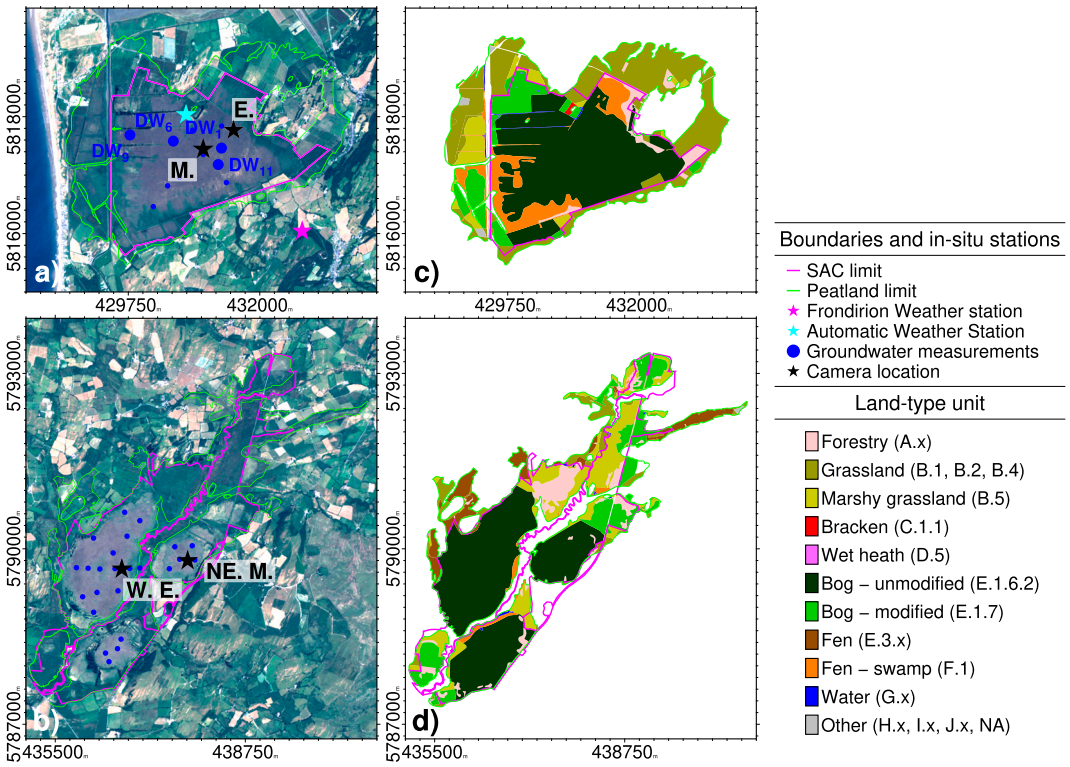

Fig. 2. Study sites. a) Natural colour satellite image of Cors Fochno (Borth bog) site from Sentinel-2 L1C (2018-06-29). b) Natural colour satellite image of Cors Caron site from Sentinel-2 L1C (2018-06-29). Camera locations are shown as black stars in each panel. At Cors Fochno, the camera stations are named: M.: Middle, E.: Edge. At Cors Caron, the camera stations are named: W. E.: West Edge and NE. M.: Northeast Middle. Groundwater level measurement stations are shown as blue dots in each panel. On Cors Fochno, the bigger labelled blue dots represent the stations discussed in the main text. c-d) Land types from the Terrestrial Phase 1 Habitat survey of Wales for both peatlands. The grids are given in UTM Zone 30 N meters. Basemap Data: Sentinel-2 imagery. Peatland-limit data: see Data availability section. (For interpretation of the references to colour in this figure legend, the reader is referred to the web version of this article.)

3. Datasets and methods

3.1. InSAR estimation of peat surface displacements

3.1.1. Space-based radar interferometry for ground surface displacements

Interferometry of Synthetic Aperture Radar (InSAR) is an active remote sensing approach for estimating ground surface displacement from radar data (Bürgmann et al., 2000; Massonnet and Feigl, 1998). The basic principle of InSAR is that a change in the phase of a back-scattered signal between two SAR image acquisitions can be directly related to a change in the distance from the radar antenna to ground surface targets (or scatterers). Thus the phase values at each respective pixel within two co-registered SAR images that were acquired on different dates are subtracted to produce an image termed an interferogram. The quality of the differential phase in the interferogram is directly controlled by the phase stability, termed InSAR coherence (or temporal decorrelation), between the two SAR acquisitions (Zebker and Villasenor, 1992).

In reality, the differential phase values in the interferogram pixels are not only proportional to the ground surface motions but are also affected by other sources of phase change, such as: orbit inaccuracy, topographic relief, atmospheric delays, and noise (Massonnet and Feigl, 1998). While orbital and topographic phase corrections are readily achieved, atmospheric phase delay presents a more difficult component to remove from an interferogram. Atmospheric effects can be non-negligible if ground motions between acquisitions are subtle (sub-centimetre). Such effects can be especially problematic in temperate or humid climates because of significant variation of atmospheric water content in space and time.

Stacking of multiple interferograms from SAR images acquired over time not only enables a timeseries of surface displacement to be obtained at each pixel but also minimises other sources of phase change, especially those related to atmospheric delays. Several approaches have been developed to isolate reliable pixels within the interferogram stack and to obtain relative displacements as measured along the satellite's line of sight (LOS). These approaches can include Permanent Scatterers® (Ferretti et al., 2011; Ferretti et al., 2001), Persistent Scatterers (Hooper, 2008), Distributed Scatterers Small-Baseline Subsets (Casu et al., 2006) or Intermittent Scatterers Small-Baseline Subsets (ISBAS) (Sowter et al., 2013). The temporal evolution of motion obtained from such approaches is given in relation to a reference date and a spatial reference point that is considered stable over the observation period. Displacement rates are estimated by fitting a linear or non-linear (e.g., quadratic) trend to the timeseries of observations. The conventional accuracy of InSAR-derived displacement measurements reaches ±5 mm for a single observation and increases to ± 1 mm·yr^{-1} for displacement rates derived from multiple observations (Hanssen, 2001).

The InSAR method has a proven ability to map ground surface displacements on various targets with different surface conditions and displacement rates (e.g., cities, volcanoes, earthquakes, landslides, etc.) (e.g., Biggs and Pritchard, 2017; Boncori, 2019; Hanssen, 2001; Hooper et al., 2012; Pinel et al., 2014; Sansosti et al., 2014). Such targets are usually characterised by high/moderate InSAR coherence. Vegetated targets commonly represent more challenging conditions for InSAR methods, due to typically low InSAR coherence (Zebker and Villasenor, 1992). Temperate raised bogs in relatively good condition have a relatively high coherence (Hrysiewicz et al., 2023), however, which allows for InSAR applications (see Supplementary Materials Figs. S2, S3 and S4). This is likely because the radar penetrates the thin mossy vegetation layer and because soil moisture changes are not too large (Hrysiewicz

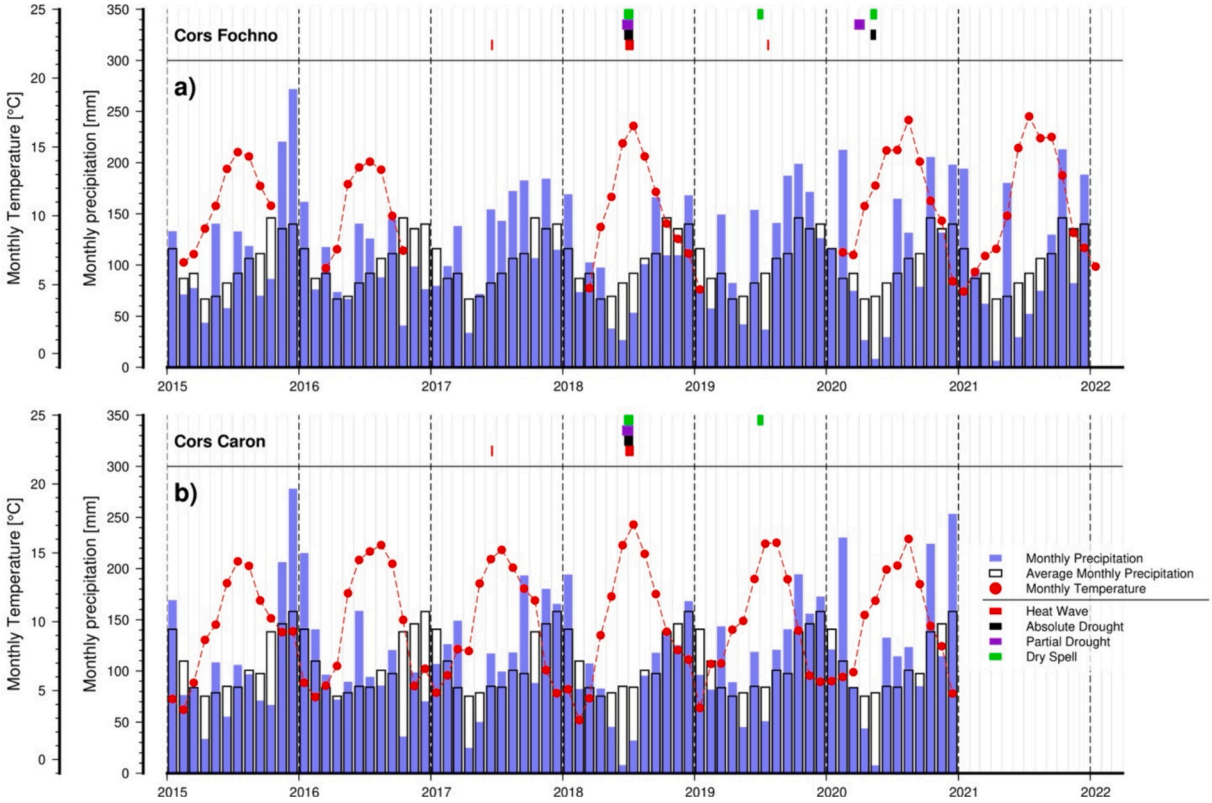

Fig. 3. Weather data for the study period 2015–2022 from HadUK-Grid and local stations. The Frondirion station is located outside the Cors Fochno area (see Fig. 1) and has measured daily rain precipitation since 1981. There is also an Automatic Weather Station (AWS) located on Cors Fochno that measures several weather parameters (i.e., daily rainfall, daily air temperature). However, there are many observation gaps with this station. For Cors Fochno, the light blue bars are the total monthly rain precipitation from data measured by the local Frondirion station, whereas the unfilled bars show the average monthly precipitation over the period 1981–2021. The red dots represent the monthly temperatures measured by the AWS. For Cors Caron, there is no local station, so the same parameters are computed from the HadUK-Grid dataset: a kilometre-scale grid of weather data interpolated from regional stations of the UK Meteorological Office. The drought periods are given at the top of both sub-figures following the UK/IE classification and the HadUK-Grid data. A heat wave is defined where daily maximum air temperature was >25.0 °C for five or more days consecutively. Absolute drought is a period of 15 consecutive days (or more) for which mean daily measured rainfall does not exceed 0.2 mm, whereas dry spell is the same period with a rainfall threshold of 1 mm. Similarly, partial drought is a period of at least 29 consecutive days where mean daily rainfall (for period) does not exceed 0.2 mm/day. (For interpretation of the references to colour in this figure legend, the reader is referred to the web version of this article.)

et al., 2023).

3.1.2. Preparation of Sentinel-1 InSAR stack

In this study, we use all available Sentinel-1 A/B data in Interferometric Wide (IW) mode, in both orbital pass directions: ascending (asc., i.e., south to north) and descending (desc., i.e., north to south). The images were acquired on Sentinel-1 Track 30 in ascending orbit and on Sentinel-1 Track 52 in descending orbit. The SAR dataset spans the period from April 2015 to March 2023, i.e., an observation period of c. 8 years. With both twin Sentinel-1 satellites operational, the temporal resolution is up to 6 days. The temporal resolution is up to 12 days when the Sentinel-1B satellite was not available: i.e., before its launch in April 2016 and after its loss in December 2021.

As the Sentinel-1 data, in Single Look Complex (SLC) format, is acquired through a Terrain Observation with Progressive Scans SAR (TOPSAR) imaging mode, a TOPSAR coregistration was performed by using the GAMMA® processor (Wegmüller et al., 2015). For coregistration and displacement computation, the reference images are from 2nd May 2019 for the ascending dataset (acquired at c. 17:57 UTC) and 28th May 2019 for the descending stack (acquired at c. 6:30 UTC), according to recent recommendations for selecting the reference dates for InSAR applications on temperate peatland (Hrysiewicz et al., 2023). We also use the precise orbits and the SRTM Digital Elevation Model (DEM) (Farr et al., 2007) to correct for orbital and topographic phase contributions. Each stack of co-registered images was then cropped to make four sub-stacks: two for Cors Fochno and two for Cors Caron (see Fig. 1 for sub-stack coverage).

3.1.3. Interferometric network designs

InSAR phase is measured at modulo 2π radians: between $-\pi$ and $+\pi$ (or 0 to 2π). This is referred to as "wrapped" phase. A crucial step named "unwrapping" allows one to get the cumulative values of phase changes between pixels with respect to a spatial or temporal reference point (e.g., Chen and Zebker, 2000, 2001; Chen and Zebker, 2002). The unwrapping can be done in 2D (only spatial dimensions) or in 3D (with the temporal dimension) (Hooper and Zebker, 2007). Importantly, unwrapping methods require continuity of pixels to solve the phase measurement ambiguity – i.e., the uncertainty regarding how many phase cycles of 2π radians occur between two pixels of interest in space or between two phase values for the same pixel in time. Unwrapping is challenging for peatlands, because significant spatial discontinuities in InSAR coherence and phase can occur on and around peatlands (see white arrows in Fig. S2 in Supplementary Materials). For example, InSAR phase and coherence can change abruptly in space when passing from the bog to adjacent rock outcrop, forest or grassland. Phase ambiguities in space can result from such sharp changes in the InSAR phase, such that phase unwrapping between pixels inside and outside the peatland is potentially subject to large errors. Phase ambiguities in time can be caused by large amplitude of displacement of the peat surface during dry to wet transitions (Marshall et al., 2022; Tampuu et al., 2023), and unwrapping

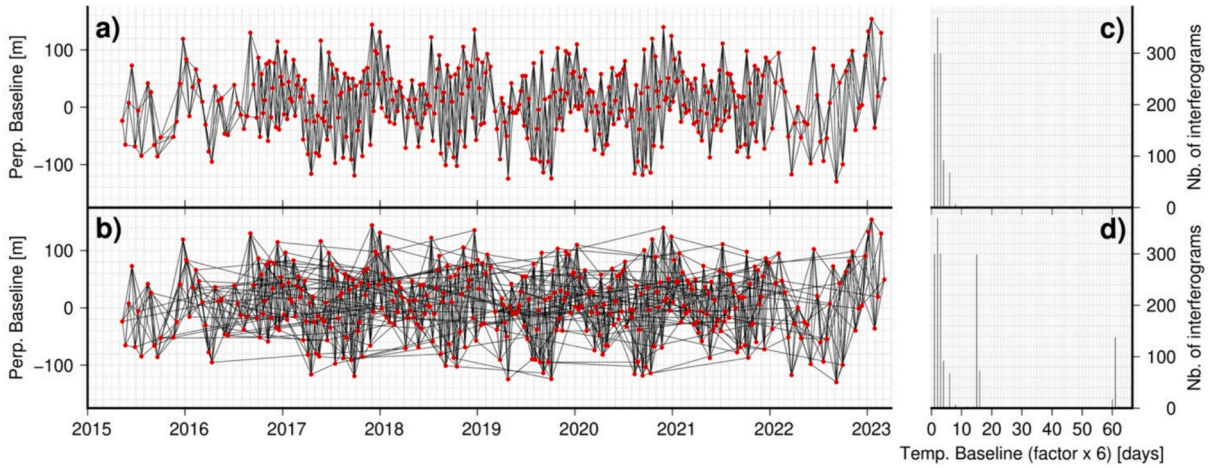

Fig. 4. Example of the two types of network of interferometric pairs used in this study. a) Network of interferograms with only the short temporal baselines. b) Network of interferograms with both long and short temporal baselines. c) Numbers of interferograms versus the temporal baselines for the "short" TBN. d) Numbers of interferograms versus the temporal baselines for the "long" TBN. See Supplementary Materials to visualise other interferometric networks tested for each sub-stack.

is further hindered by low InSAR coherence in time of lands around the peat soils during these periods (Hrysiewicz et al., 2023) (see also Supplementary Figs. S3 and S4).

The expected time-series of displacement on a raised peatland will ideally comprise a long-term (8-year) linear or quadratic component and a short-term (annual) oscillatory component. To estimate multi-annual surface displacement rates correctly, "long-temporal-baseline" interferograms spanning a 1-year period are needed to minimise the potential biases of InSAR phase arising from the interferogram network (Ansari et al., 2021). Although raised peatlands in good condition can yield 1-year interferograms with moderate to high InSAR coherence (see Fig. S3 in Supplementary Materials) (Hrysiewicz et al., 2023), interferometric pairs such with such a long temporal baseline can be strongly affected by phase ambiguity (Marshall et al., 2022; Tampuu et al., 2023). To mitigate the phase ambiguities, a network of "short-term" interferometric pairs of high InSAR coherence can be used. In such a network, each interferogram has a low probability of being affected by phase ambiguity, but multi-annual displacement rates are not accurate because of network bias (Ansari et al., 2021). Therefore, in a scenario where surface motion is characterised by relatively large short-term oscillations superimposed on a long-term linear trend, such as expected on peatlands, it is difficult to estimate accurately both the short-term displacements and the long-term displacement rates by using a single network of interferograms.

Knowing these limitations, we designed two types of network to constrain the different components of the peatland surface motions. The two networks comprise: (1): a "short" temporal baseline network (TBN), in which an image acquired on date N is connected to the successive N + 1, N + 2 and N + 3 images in the set of SLC images (Fig. 4a), to calculate shorter-term motions and (2) a "long" TBN (Ansari et al., 2021; Thollard et al., 2021) to estimate the multi-annual rate of peat surface displacement (Fig. 4b). The long TBN contains the same interferograms as the short TBN, but additionally contains interferograms with temporal baselines of 90 days and 360 days (Fig. 4c,d and supplementary Figs. S5-S8).

3.1.4. Time series analysis of peat surface displacements

The novelty of the methodological approach presented here is in the combination of the time-series results of the long TBN and the short TBN for each interferogram sub-stack (Fig. 5). Firstly, by using a long TBN, we obtain time series of InSAR-derived LOS displacements from which the longer-term multi-annual displacement rates should be correctly estimated, but from which annual displacement oscillations are underestimated due to phase ambiguities (especially during dry periods). Secondly, the high-coherence pixels identified from the long TBN are also identified as high-coherence pixels from the corresponding short TBN. Therefore, the estimation of displacements from the short TBN is made on the point distributions computed from the long TBN. Thirdly, we obtain time series of InSAR-derived LOS displacements by using the short TBNs, (see Fig. 5), for which the annual oscillations in displacement are correctly estimated but the long-term displacement rates are affected by phase biases (Ansari et al., 2021).

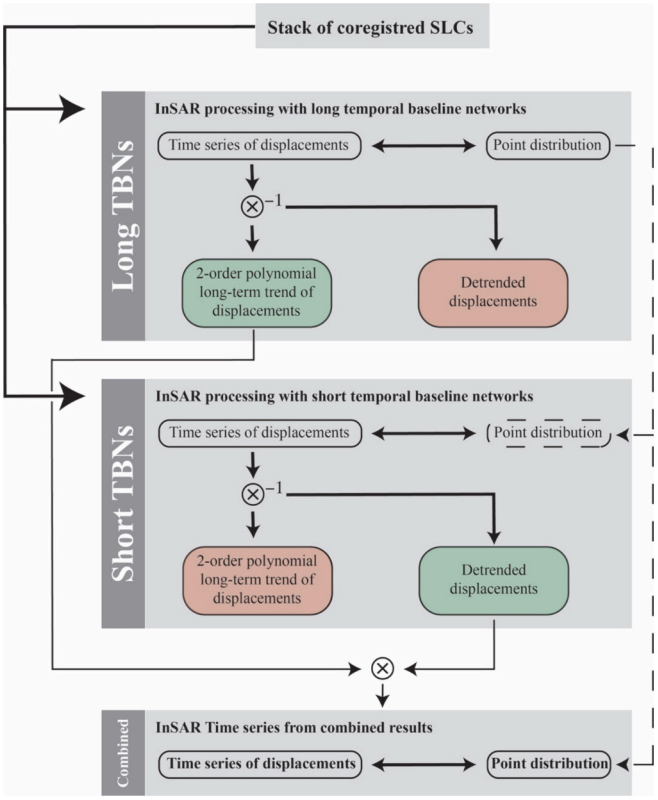

Fig. 5. Workflow for the combined TBN computation of peatland surface displacements. The green results are correctly estimated and the red results are biased. (For interpretation of the references to colour in this figure legend, the reader is referred to the web version of this article.)

The approach therefore is based on our ability to separate the long-term behaviour of displacements from the short-term behaviour. We select the correctly-estimated part of time series by using a separation based on 2-order polynomial trends: (1) the long-term displacements are estimated by the fit obtained via 2-order polynomial trends applied to the results of long TBN; (2) the short-term displacements are estimated by subtracting long-term trends constrained via 2-order polynomial equations from the results of short TBN. Finally, we create a "combined" dataset of LOS displacements for which the longer-term displacement trend is that estimated from the long TBN and the shorter-term displacement variations are those estimated from the short TBN.

Extraction of displacement time-series from each sub-stack is performed via the Interferometric Point Target Analysis® (IPTA) approach for multi-reference interferogram networks (Wegmüller et al., 2004; Werner et al., 2003). Single-looked (i.e., full resolution) and multilooked phases are used in our processing. Multilooked phases (phases averaged across several pixels) are estimated by a moving window averaging of phase values across 15 pixels in the range direction and 3 pixels in the azimuth direction. In most InSAR approaches, the selection of high-quality points, in terms of uncertainty, is based on the InSAR coherence or proxies such as temporal coherence (average coherence over time). For InSAR approaches with modelling of the phase, as in the IPTA or Permanent Scatterers approaches, the selection also can be supported by modelled phase uncertainty. In our study, only the pixels with low uncertainty, directly linked to the InSAR coherence, were analysed within the IPTA processing networks (see Supplementary Material for the list of used parameters) (Wegmüller et al., 2004; Werner et al., 2003). This selection is equivalent to a minimum coherence threshold of c. 0.3–0.4 for the full image stack. Phases were converted to displacements independently for each peatland and each data sub-stack. The reference point/area for Cors Fochno is in the town of *Tal-y-Bont* and for Cors Caron it lies in the town of *Tregaron* (see Fig. 1). The same parameters and same reference points are used for all computations on each peatland and therefore are identical (key parameters of the IPTA processing in Table S1 are in the Supplementary Materials).

3.1.5. Inversion of vertical and horizontal motions

After obtaining the combined time-series datasets from the ascending and descending tracks, vertical and horizontal (West-East) displacement components are estimated for each peatland by assuming that the South-North component of displacement is negligible (Wright, 2004). Given that the spatial resolution of the multi-looked pixels is ~40 × 60 m, we define a new regular grid (UTM Zone 30 N or EPSG:32630) for each bog at 50-m resolution. In most grid cells for coherent areas, we have points for both ascending and descending datasets. In some cells, we have one point from only one dataset or no point: such cells are considered as empty cells. If such an empty cell is surrounded by grid cells with InSAR points from both ascending and descending datasets, we still add this cell as a valid grid cell. Then the LOS displacements are spatially interpolated on the grid by using the natural-neighbour interpolation method. This method allows a smoother interpolation compared to nearest-neighbour method (Amidror, 2002). The LOS displacements are temporally interpolated on the dates of the ascending datasets by using a piecewise cubic Hermite polynomial interpolation method (Fritsch and Carlson, 1980; Kahaner et al., 1989) because of an average 2-day delay between ascending and descending acquisitions and because of the ability of this method to minimise the noise reduction by shape preservation. The vertical and horizontal displacements are estimated by least squares inversion, and the linear displacement rates are recomputed for the vertical and horizontal components. The acquisition dates of the ascending data are used as the sampling dates for the final timeseries. Uncertainties of displacement on each date are estimated by using the standard deviation values of displacements for the points in the spatial reference areas (see Fig. 1).

3.2. In-situ data for peat surface motions, groundwater levels and peat thickness

The instrument for in-situ measurement of peat surface motion comprises a digital camera module mounted on a lightweight platform that is pinned to the peat surface (Evans et al., 2021a). A 20-mm diameter subsidence pole made of galvanised steel passes through the camera platform and is anchored within the peat body, and ideally within the sub-peat mineral soil: i.e., Cors Fochno peat cameras are anchored in the clay layer (see Fig. 6). The camera is focussed on a graduated ruler with ArUco (image recognition) markers fixed to the pole. Motion of the camera, and thus of the peatland surface, is with respect to the stable subsidence pole. The surface displacement is calculated automatically by digital image correlation. The precision of the measurements is sub-mm, and the accuracy is better than 10 mm, which is the value of RMSE between the peat-camera measurements and manual subsidence pole measurements of Evans et al. (2021a). The temporal resolution is daily (for Cors Fochno) or sub-daily (for Cors Caron). Although deployed here in relatively accessible peatlands, the instrumentation can be adapted for more difficult logistical conditions (e.g., by using PVC pipes instead of metal hollow tubes to reduce weight for transport) and has been successfully deployed to remote locations from Indonesian swamp forests (Evans et al., 2021a) to exposed upland areas of the Falkland Islands, where they have run autonomously for up to a year.

The peat-camera measurements cover a roughly 2.5-year period from late-2019 to mid- or late-2022. Cors Fochno is equipped with two camera stations named Middle (observation period: Feb. 2020 – Sept. 2022) and Edge (observation period: Feb. 2020 – Jun. 2021) (Fig. 2a and b). The peat thickness at each peat-camera location is around 7 m and 8 m, respectively. Cors Caron has two peat camera stations, named West Edge and Northeast Middle, that were working between Sept. 2019 and mid-2022 in the areas for which we have InSAR results (Fig. 2b). Peat thickness near the West Edge camera is around 6 m (Godwin and Mitchell, 1938), while peat thickness at the Northeast Middle camera location is not well defined but is likely around 6–9 m. Regarding the in-situ measurements of displacements, two assumptions are made in this study: (1) uncertainties associated with peat-camera measurements are negligible compared to InSAR-derived displacements; (2) there is no

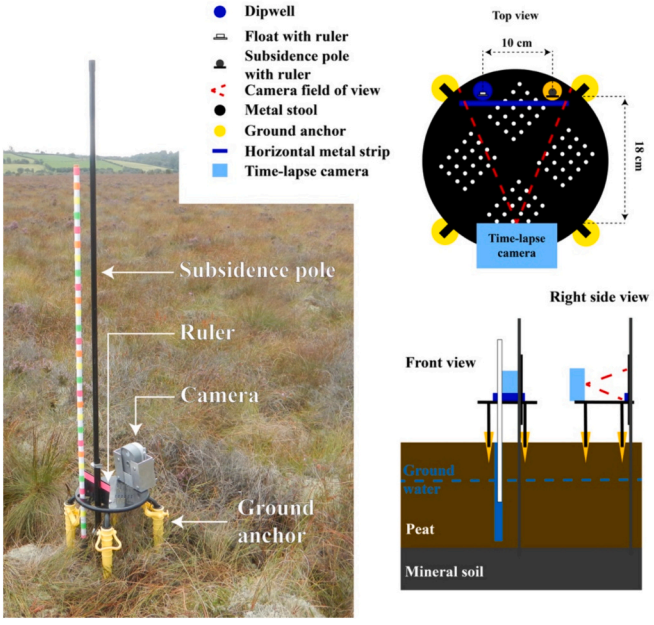

Fig. 6. Picture of a peat camera installed on Cors Fochno, with the associated description. Modified from (Evans et al., 2021a).

sustained impact on the in-situ displacement time series (i.e., step change) from site visits to replace batteries and retrieve data. The daily averages of all the peat camera time series were calculated in order to maintain the consistency of the in-situ time series.

Cors Fochno is equipped with 11 dip wells – named DW for Dip Well (see Fig. 2a) – each of 1-m length and 36-mm internal diameter. The wells are fixed via a steel pole driven into the basal clay. Water levels are measured with SOLINST® Levelogger 5 and referenced to a standardised peatland surface for each well. The standard surface is based on the mean of peatland surface elevation measurements made at 33 points within a 2-m radius of each dip well after its installation. The purpose of this metric is to take into account the microtopography of the bog surface around each dip well, and to avoid inaccuracies regarding the asynchronous motions between peat surface and tubes. On the three domes of Cors Caron (see Fig. 2b), 21 "floating" dip wells – named CC for Cors Caron – have been installed (i.e., floating along with the peat, and hence providing data relative to the peat surface). Each dip well comprises a tube of 1-m length and contains a SOLINST® Levelogger 5, suspended usually around 70–80 cm below the peat surface.

Peat thickness data for Cors Fochno are derived from ground penetrating radar profiling conducted in 2009. Those for Cors Caron are derived from probing in winter 2020/2021. The peat surface elevation of both bogs is taken from the 2020–2022 Wales Lidar DSM at 1-m resolution.

3.3. Statistical methods to compare the in-situ measurements and InSAR-derived time series

The difference in temporal sampling of displacement obtained through the InSAR (e.g., 6–12 days) and the peat cameras (i.e., sub-daily) requires defining a robust workflow for their comparison. Two aspects of peat surface motion are compared in this study: (1) the linear displacement rate (velocity) and (2) the oscillatory displacement time series.

The peat surface displacement rates are calculated by least-squares inversion from each time series over their common observation periods only. Uncertainties are considered to be homogeneous for each InSAR-derived observation. For comparing their displacement rates to those from either the ascending or descending passes, the vertical displacements from the peat cameras are converted to those expected in the satellite LOS by a multiplication factor of $\frac{1}{cos\ (inc)}$, where *inc* is the incidence angle (Wright, 2004). The mismatch (or offset), in mm·yr^{-1}, is calculated from the RMSE weighted by velocity uncertainty:

$$RMSE(X,Y) = \sqrt{\frac{\sum_{i=1}^{n} W_i (Y_i - X_i)^2}{\sum_{i=1}^{n} W_i}}, \quad (1)$$

with n the number of points, X_i the in-situ peat-surface-motion velocity, Y_i, the InSAR-derived peat-surface velocity and W_i the weight of each point (York, 1968), where

$$W_i = \frac{\omega(X_i)\omega(Y_i)}{\omega(X_i) + \omega(Y_i) - \alpha}, \quad (2)$$

and where the term ω corresponds to the weight defined as the inverse of the variance (uncertainties at power 2) for the observation i. In most cases, the term α can be negligible, as it corresponds to the error correlation. Here α is non-negligible however, since the velocity uncertainties are caused by the annual oscillations of displacement, inducing potential correlations of uncertainties. α is therefore defined as $2r\sqrt{\omega(X_i)\omega(Y_i)}$, with r the Pearson's correlation coefficient of uncertainties (York, 1968). This coefficient is defined as follows:

$$r(X,Y) = \frac{1}{n}\sum_{i=1}^{n}\left(\frac{X_i - \mu_X}{\sigma_X}\right)\left(\frac{Y_i - \mu_Y}{\sigma_Y}\right), \quad (3)$$

with μ_X and μ_Y the mean values of X and Y, σ_X and σ_Y the standard deviation values of X and Y.

For point-wise comparison of the displacement time series, we select Pearson's correlation coefficient as the estimator (see Eq. 3). First, the in-situ peat camera measurements are interpolated onto the SAR-data temporal dates by using a piecewise cubic Hermite polynomial interpolation method (Fritsch and Carlson, 1980; Kahaner et al., 1989) to reduce the in-situ sampling rate from a daily frequency to 6/12 day frequency. The in-situ and InSAR time series are then cut to retain only the data from the overlapping observation periods, and they are detrended by assuming a linear long-term displacement trend and homogenous uncertainties. Then Pearson's correlation coefficients are calculated. This coefficient is suitable to quantify the similarity of each time series with regard to the periodicity of the annual peat-surface-motion oscillations. In addition, the RMSE, without weight, is computed for the same time series in order to quantify the differences in the amplitude of oscillations.

Temporal interpolation is required also for the groundwater level time series to comply with the sampling rate of the InSAR results. The piecewise cubic Hermite polynomial interpolation method is also used in this case (Fritsch and Carlson, 1980; Kahaner et al., 1989).

4. Results

4.1. InSAR-derived displacements from long and short temporal baseline networks

4.1.1. Long temporal baseline networks

The number and density of good quality InSAR points are highest on each "unmodified" peat dome, with points also retrieved on some 'modified' bog areas (Fig. 7). In general, point density decreases outward from the dome centre, where there is near complete coverage, to the bog edges, where there are isolated points. Few or no good quality InSAR points are obtained for the peat soil areas classed as swamp, fen, woodland, marshy grassland or grassland (Fig. 2). The extended displacement rate maps for the areas around the bogs, can be found in Supplementary Materials (see Figs. S9 and S10). InSAR points outside of the SACs are mainly obtained on man-made structures (i.e., villages, farm buildings, railway lines, roads, etc.).

On Cors Fochno, the long TBN results indicate that during the full observation period the centre of dome had negative LOS displacements, at rates of up to ~ -6 mm·yr^{-1} (see Fig. 7a-b). The dome edges, conversely, had positive LOS displacement rates of up to $\sim +4$ mm·yr^{-1}, with maximum values in the north-west. The LOS displacement pattern is not perfectly centred on the bog: it is offset to north-east. LOS displacement rates obtained from the ascending and descending passes are broadly similar, an observation compatible with mainly vertical displacement of the bog surface as the incidence angles of the SAR geometries differ by only a few degrees (ascending: 34°; descending: 39°) (see Table 1).

For Cors Caron, the long TBN results indicate that the bog had entirely negative LOS displacement rates, with a rate of ~ -8 mm·yr^{-1} in the bog centre (see Fig. 7c-d). As for Cors Fochno, the LOS displacement rate decreases toward the margins, but with only a few points of positive displacement rate in the northeast of the western peat unit. For the north-western peat dome, the maximum LOS displacement rate pattern was also not centred on the bog but shifted toward the north-western border. Results on the bog complex from the ascending and descending passes are again broadly similar (see Table 1).

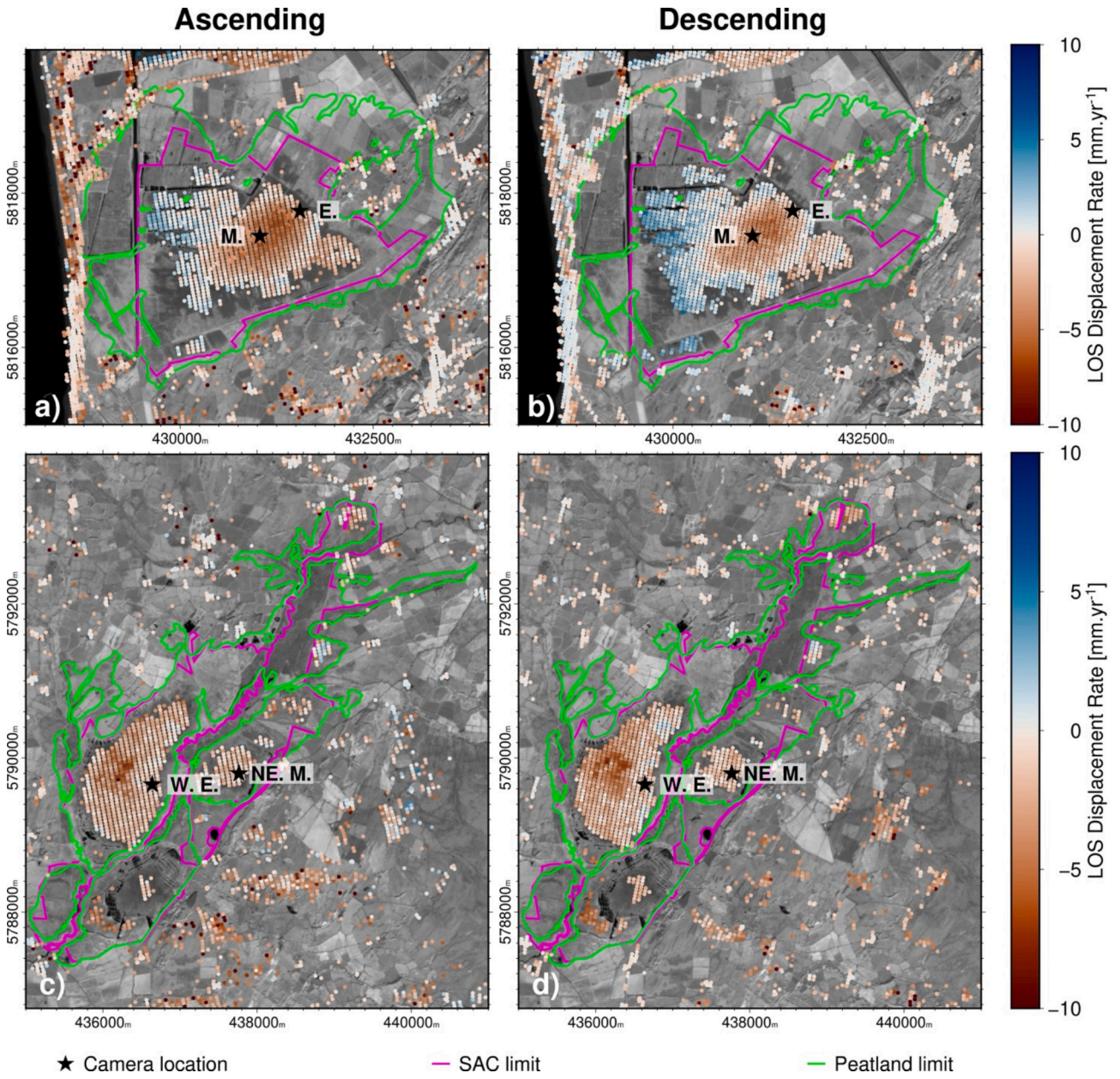

Fig. 7. InSAR-derived LOS displacement maps for the two raised peatlands from the long TBNs. a) Map of InSAR-derived LOS displacement rate at Cors Fochno for the ascending pass, and b) Map of LOS displacement rate at Cors Fochno for the descending pass. c) Map of InSAR-derived LOS displacement rate at Cors Caron, for the ascending pass. d) Maps of LOS displacement rate at Cors Caron for the descending pass. The maps are given in UTM Zone 30 N meters. Peat-camera locations are shown as black stars in each panel. The names of peat-camera stations are for Cors Fochno: M.: Middle, E.: Edge; and for Cors Caron: W. E.: West Edge and NE. M.: Northeast Middle. Basemap Data: near-infrared reflectance image (Band 8) from Sentinel-2 L1C (2018-06-29). Peatland-limit data: see Data availability section.

4.1.2. Short temporal baseline networks

InSAR-derived displacement rates on the bogs computed from the short TBNs show an increase in spatial noise compared to those from the long TBNs (see Fig. 8). Although the short and long TBNs yielded broadly the same displacement rates for Cors Fochno (see Table 1), the short TBN yielded significantly greater LOS displacement rates of up to 15 mm·yr^{-1} for Cors Caron compared to rates of up to 5 mm·yr^{-1} from the long-TBNs (see Table 1).

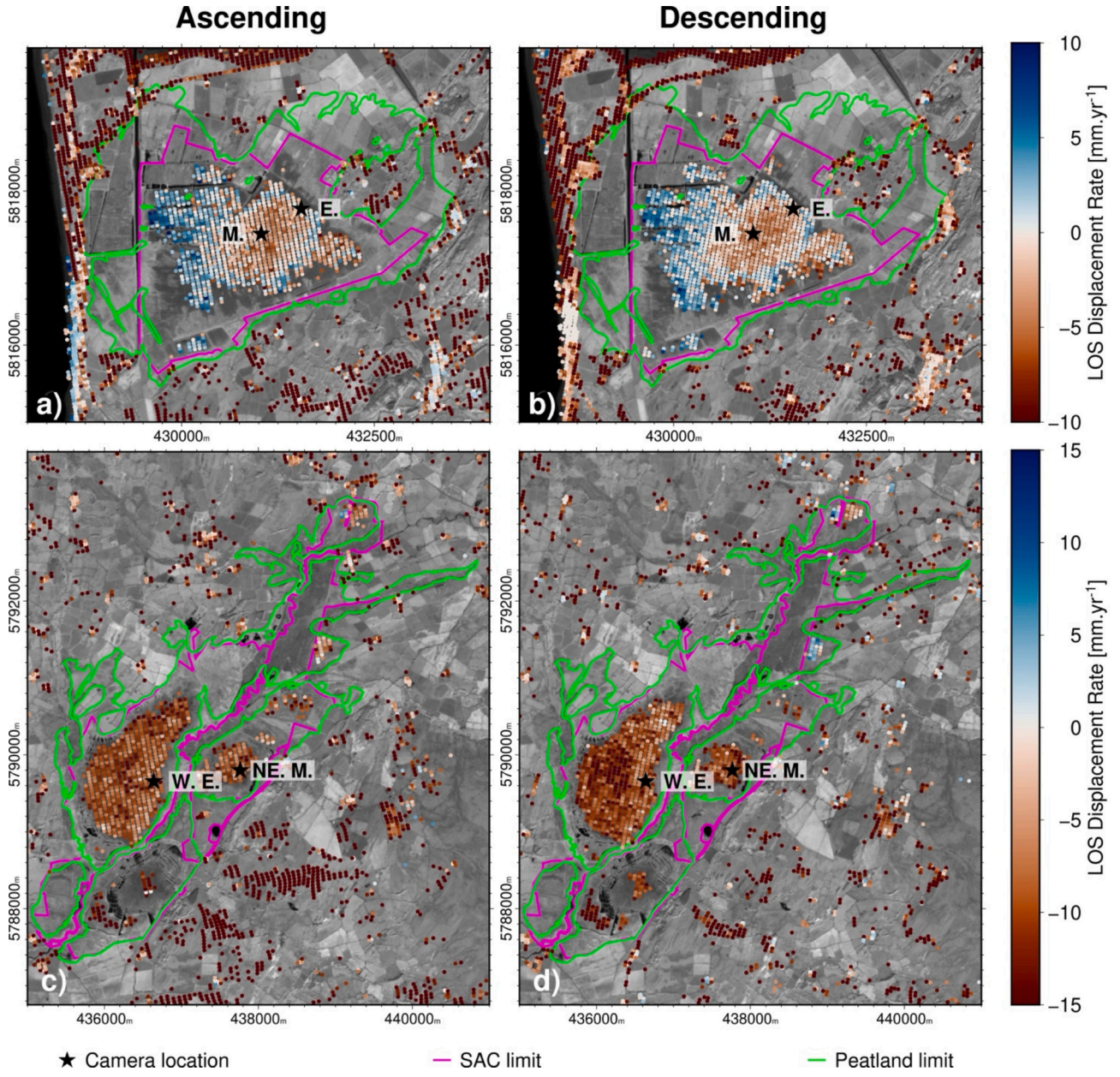

Fig. 8. InSAR-derived LOS displacement maps for the two raised peatlands from the short TBNs. a) Map of InSAR-derived LOS displacement rate at Cors Fochno for the ascending pass. b) Map of LOS displacement rate at Cors Fochno for the descending pass. c) Map of InSAR-derived LOS displacement rate at Cors Caron, for the ascending pass. d) Maps of LOS displacement rate at Cors Caron for the descending pass. The maps are given in UTM Zone 30 N meters. Peat-camera locations are shown as black stars in each panel. The names of peat-camera stations are for Cors Fochno: M.: Middle, E.: Edge; and for Cors Caron: W. E.: West Edge and NE. M.: Northeast Middle. Basemap Data: near-infrared reflectance image (Band 8) from Sentinel-2 L1C (2018-06-29). Peatland-limit data: see Data availability section.

Table 1
Overview of average InSAR-derived displacement rates in mm·yr^{-1} computed on Cors Fochno (C.F.) and Cors Caron (C·C.) for long- and short-temporal baselines of interferograms. Standard deviations are given at 1σ.

	Long TBN		Short TBN	
	Ascending	*Descending*	*Ascending*	*Descending*
Mean LOS velocity on C.F.	−1.4 ± 2.1	−0.3 ± 2.1	−0.2 ± 3.2	−0.3 ± 2.1
Mean LOS velocity on C.C.	−2.1 ± 1.4	−2.1 ± 1.6	−9.2 ± 3.1	−10.0 ± 3.5
Mean LOS velocity around C.F.	−2.2 ± 4.3	−0.6 ± 2.4	−13.2 ± 10.7	−8.2 ± 9.5
Mean LOS velocity around C.C	−1.8 ± 4.0	−1.3 ± 2.2	−12.0 ± 10.8	−6.6 ± 9.5

Another key difference between the short and long TBN results concerns the displacement rates estimated outside the bogs, i.e. in those areas not mapped as underlain by peat soil. While average LOS displacement rates from the long TBNs inside and outside the bogs are similar, the average rates for outside the bogs from the short TBNs are strongly biased toward much more negative values (see Fig. 7 vs Fig. 8, Table 1 and Figs. S9, S10 and S11 in Supplementary Materials).

4.1.3. Comparison of long and short TBNs with in-situ displacements over the bogs

At both study sites, the peat cameras show that the bog surface oscillates annually, with the peat surface elevation higher in winter and lower in summer (red points in Fig. 9). At Cors Fochno, the amplitude of oscillation is around ±20 mm (see Fig. 9a-d); at Cors Caron, the amplitude is around ±10 mm (see Fig. 9e-h). Based on a linear fit, the Middle peat camera at Cors Fochno showed a c. 3-year surface motion rate of -18 ± 0.5 (1σ) mm·yr^{-1}, while 3-year motion rates for the Cors

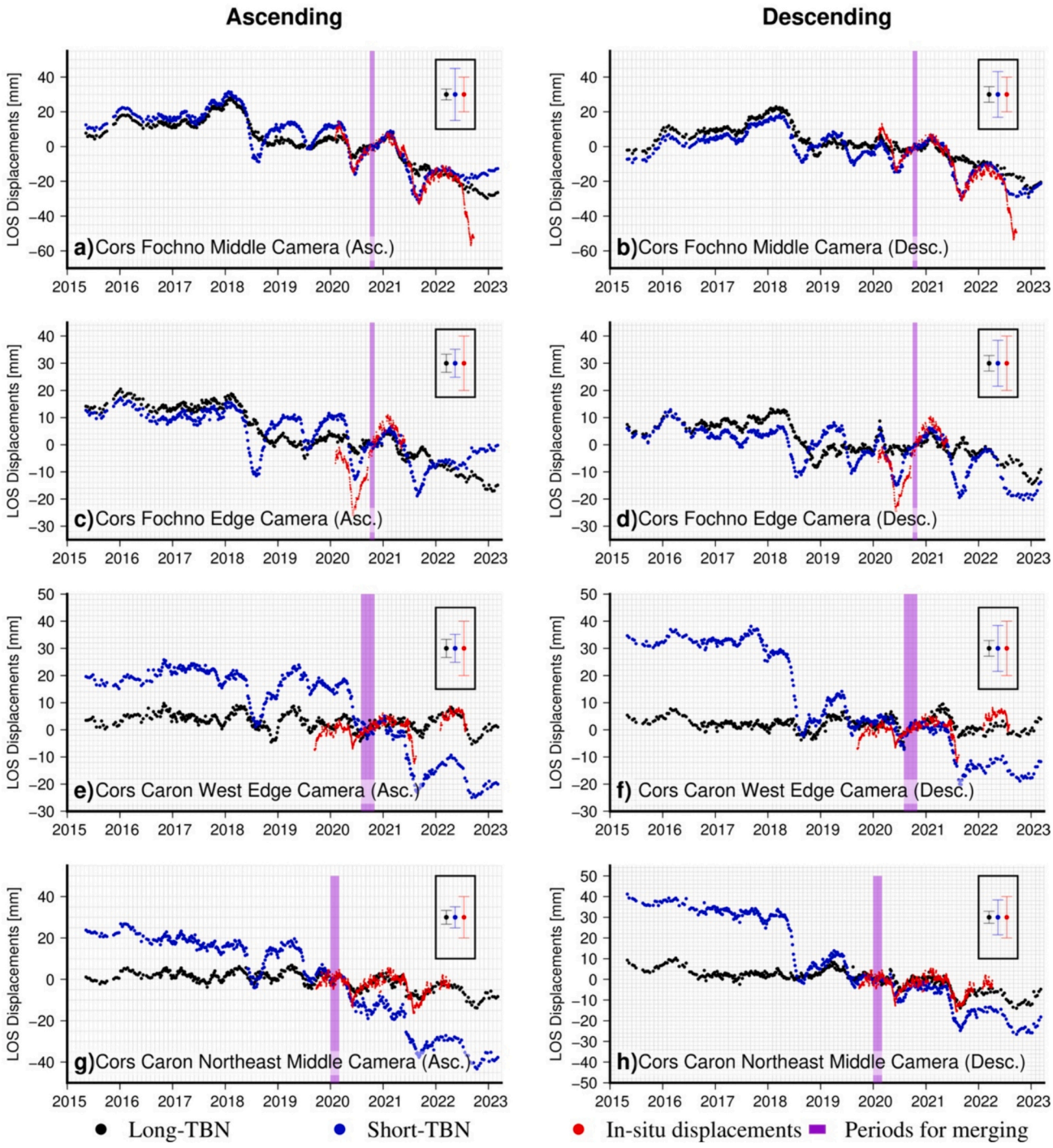

Fig. 9. Time series of InSAR and in-situ LOS displacements. a)-g) Times series of LOS displacements for all the used peat-camera stations (red) with the time series computed from long- and short-temporal-baseline networks (black and blue, respectively). Error bars give the mean of uncertainties. The purple polygons give the periods used to merge both relative time series. Asc.: ascending. Desc.: descending. (For interpretation of the references to colour in this figure legend, the reader is referred to the web version of this article.)

Table 2
Overview of InSAR-derived LOS displacement times series parameters computed on Cors Fochno (C.F.) and Cors Caron (C.C.) with either a short or a long temporal baseline network (TBN). The velocities at the peat camera locations are estimated for the durations of peat-camera time-series. Standard deviations are given at 1σ. Pearson's coefficients and RMSE for the correlation between InSAR LOS displacements and in-situ measurements projected into the satellite LOS are given also. The *p-values* of correlations coefficients are lower than 0.001.

	Long TBN		Short TBN	
	Ascending	*Descending*	*Ascending*	*Descending*
C.F. Middle	−10.7 ± 0.6	−6.8 ± 0.3	−11.0 ± 1.1	−8.5 ± 1.0
C.F. Edge	−1.0 ± 0.7	0.5 ± 0.8	−0.5 ± 1.8	9.0 ± 1.5
C.C. West Edge	0.8 ± 0.2	−0.4 ± 0.3	−15.0 ± 0.6	−7.8 ± 0.5
C.C. Northeast Middle	−2.8 ± 0.4	−4.1 ± 0.4	−16.8 ± 0.5	−8.3 ± 0.5
Mean RMSE [mm·yr^{-1}]	**5.2**		**12.5**	
C.F. Middle	0.73 / 6.44	0.55 / 7.15	0.76 / 6.11	0.90 / 3.53
C.F. Edge	0.72 / 5.90	0.61 / 5.87	0.89 / 3.44	0.87 / 3.63
C.C. West Edge	0.52 / 3.80	0.41 / 3.96	0.76 / 3.46	0.78 / 2.85
C.C. Northeast Middle	0.76 / 2.79	0.73 / 2.75	0.80 / 2.76	0.84 / 2.39
Mean coefficient and RMSE [mm]	**0.63 / 4.83**		**0.83 / 3.52**	

Caron West Edge and Northeast Middle peat cameras were 2.9 ± 0.2 mm·yr^{-1} and -2.4 ± 0.3 mm·yr^{-1}, respectively. The linear motion rate for the Cors Fochno Edge peat camera was +18.8 ± 1.3 mm·yr^{-1}, but, because the measurement period is just over one year, one must treat this estimate with caution.

The InSAR-derived LOS displacement rates for the peat camera locations differ depending on the interferogram network used (Fig. 9). For the two peatlands, the lowest average mismatch (RMSE) of velocity for InSAR versus peat camera is obtained by using the long TBNs. The RMSE for the long TBN is 5.2 mm·yr^{-1}, whereas that for the short TBN is 12.5 mm·yr^{-1} (see the upper part of Table 2). Consequently, and as expected, the long TBNs appear to be the best interferometric networks to estimate the multi-annual rates of peat surface displacements.

On the other hand, the InSAR time series from long TBNs show systematic underestimation of displacement oscillations as measured in-situ. Instead, the InSAR time series from short TBNs better match the annual oscillations of the in-situ displacements (see Fig. 9). The Pearson's coefficient is used to define the correlation between the detrended InSAR-derived observations and the detrended in-situ measurements (see the lower part of Table 2). For the two peatlands, the highest coefficient and lowest RMSE are obtained by the short TBNs, demonstrating that these networks capture the periodicity of displacement oscillations. For the amplitude, the same networks give the lowest RMSE. Consequently, and again as expected, the short TNBs appear to be the best interferometric networks to estimate the sub-annual oscillation of peat surface displacement.

4.2. InSAR results from combined long and short TBNs

While the long-TBN results give accurate estimates of the multi-annual surface motion velocity, the short TBNs capture with the best accuracy the amplitude of sub-annual oscillations. Therefore, we create combined results for which: (1) the long-term LOS velocity is estimated by using the long TBNs; (2) the LOS displacements are estimated by using the short TBNs. Then, these combined datasets are used to compute the vertical (Up-Down) and horizontal (East-West) components of displacements. After fusion of the ascending and descending data, the coverage of InSAR measurement points is reduced on the regional scale to 50 and 17 points per km^2 for the Cors Fochno and Cors Caron areas, respectively. On the two peatlands, however, the point density remains high at ~180 points per km^2 for Cors Fochno and ~ 140 points per km^2 for Cors Caron. In the following sections, all shown displacements and displacement rates are from the combined TBN datasets.

4.2.1. Vertical and horizontal components of multi-annual ground motion rate

On Cors Fochno, the combined TBN InSAR results indicate that during the observation period the centre of bog area has undergone subsidence at rates of −7 mm·yr^{-1} (see Fig. 10a). The bog edges have conversely undergone uplift of up to +5 mm·yr^{-1}, with maximum values in the north-west. As seen for the LOS displacements (Fig. 7 and Fig. 8), the vertical displacement pattern is not perfectly centred on the bog: it is offset to north-east. The combined TBN results also indicate an apparently consistent if small eastward component of long-term displacement on Cors Fochno (see Fig. 10b), but these apparent horizontal displacements may not be significant as their statistical distribution is 0.85 ± 0.60 (1σ) mm·yr^{-1}. This is confirmed by the very high similarity of displacements from each pass during our computations from long-temporal-baseline networks, with similar incidence angles of the SAR geometries. Further details on horizontal displacements at peat camera locations can be found in Supplementatry Materials (Fig. S12).

For Cors Caron, the combined TBN InSAR results indicates that almost the entire bog has undergone subsidence, at up to a rate of −9 mm·yr^{-1} (see Fig. 10c). The vertical displacement rate decreases toward the margins, but little or no uplift is observed. For the north-western unit, the vertical displacement rate pattern is also not centred on the bog but shifted toward the north-western border. Again, we do not observe significant horizontal displacement (Fig. 10d) given the noisiness of the patterns in space and the measurement uncertainty (−0.13 ± 0.90 (1σ) mm·yr^{-1}). Further details on horizontal displacements at peat camera locations can be found in Supplementary Materials (Fig. S12).

Around the camera stations, the linear approximation of the combined TBN InSAR time series yields long term (i.e., ~8 years) subsidence rates, at 1σ, of: −5.4 ± 0.3 mm·yr^{-1} (Fig. 11a); −4 ± 0.2 mm·yr^{-1} (Fig. 11b); −0.8 ± 0.1 mm·yr^{-1} (Fig. 11c); and − 1.8 ± 0.1 mm·yr^{-1} (Fig. 11d) (respectively Cors Fochno Middle, Cors Fochno Edge, Cors Caron West Edge and Cors Caron Northeast Middle). In detail, however, there is considerable non-linearity to the displacement evolution with time at both bogs. In the medium term (i.e., ~3 years), Cors Fochno and Cors Caron display subsidence or uplift trends either side of the summer of 2018. At Cors Fochno, the bog centre appears to have uplifted at ~ + 5 mm·yr^{-1} during 2015–2018, after which it appears to have subsided at around −8 mm·yr^{-1} during 2019–2023. At Cors Caron, the medium-term displacement rates around the camera stations show apparent uplift between 2015 and 2018. On the short term (i.e., ~1 year), the InSAR data also show seasonal oscillations of typically ±5–20 mm, but with up to ±30 mm reached at Cors Fochno in summer 2018.

4.2.2. InSAR time series versus in-situ camera measurements

The in-situ peat camera data show good agreement with the combined TBN InSAR data in terms of the phase, period and amplitude of the annual (seasonal) oscillations (Fig. 11). The amplitude of surface oscillation as measured by InSAR is well matched to the in-situ data for the middle cameras on each bog. The surface oscillation amplitude is underestimated by InSAR for the edge cameras on each bog, especially for the Cors Fochno Edge PeatCam station (maximum mismatch of 15 mm in the 2020 summer season). The average mismatch (RMSE) of the InSAR and in-situ velocities for all the stations is 7.1 mm·yr^{-1} (Table 3). Given that the medium-term rate of motion can be strongly affected by shorter-term variation and the length of the observation period, it is noteworthy that the average mismatch for the in-situ and InSAR motion rates decreases to 4.5 mm·yr^{-1} if the shorter-term Cors Fochno Edge

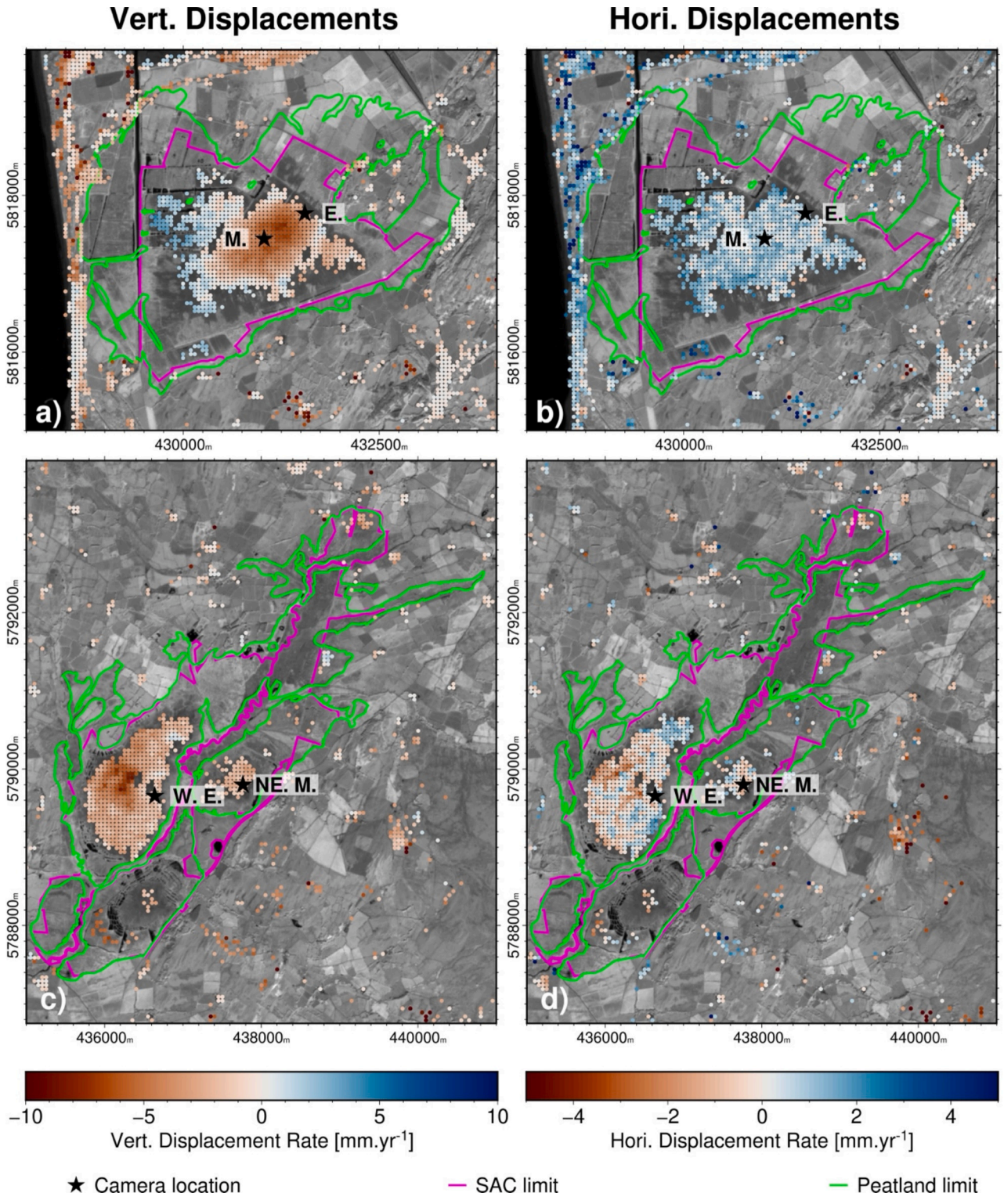

Fig. 10. InSAR-derived displacement maps for the two raised peatlands. a) Map of InSAR-derived vertical displacement rate at Cors Fochno, and b) Map of horizontal (West-East) displacement rate at Cors Fochno. c) Map of InSAR-derived vertical displacement rate at Cors Caron. d) Horizontal (West-East) displacement rate at Cors Caron. The maps are given in UTM Zone 30 N. Negative vertical displacement implies subsidence; Negative horizontal displacement implies westward motion. Peat-camera locations are shown as black stars in each panel. The names of peat-camera stations are for Cors Fochno: M.: Middle, E.: Edge; and for Cors Caron: W. E.: West Edge and NE. M.: Northeast Middle. Basemap Data: near-infrared reflectance image (Band 8) from Sentinel-2 L1C (2018-06-29). Peatland-limit data: see Data availability section.

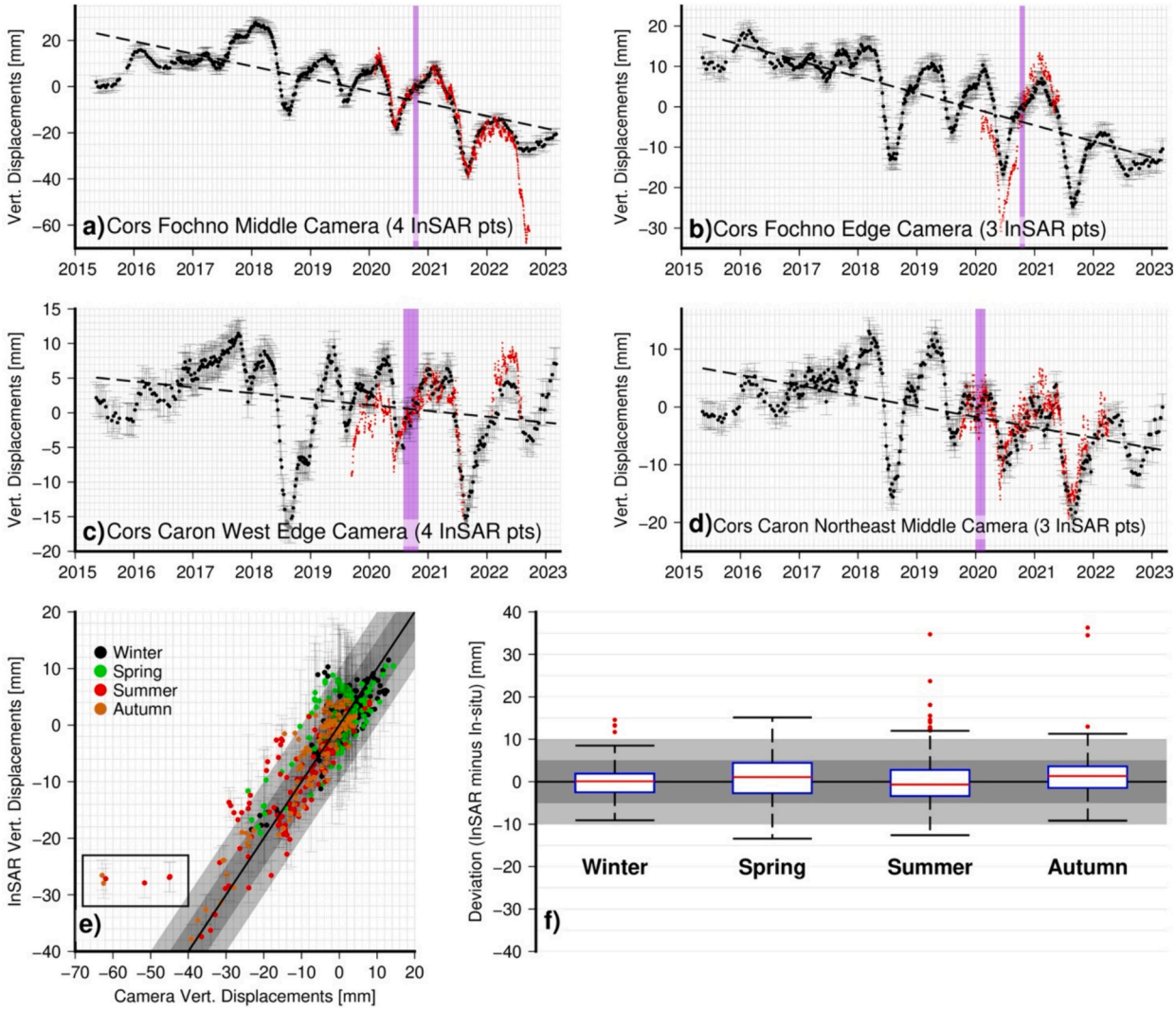

Fig. 11. Time series of InSAR and in-situ vertical displacements. a)-d) Times series of vertical displacements in the vicinity of each peat camera station. The InSAR-derived results are represented by black dots and in-situ with red dots. The long-term trends are represented by black dashed lines. The purple vertical bars give the periods used to merge the time series. A brief description of horizontal displacements is given in Supplementary Materials. The peat camera data cover the period from late-2019 to mid-2022, while the InSAR measurements – here reported for the area with a radius of 50 m of each peat camera location – span the years 2015 – mid-2023. e) Correlation plot between InSAR-derived and in-situ displacements, classified by season. The black box highlights the outliners linked to the time series of Cors Fochno Middle. f) Boxplots of deviations (InSAR displacements minus in-situ displacements), classified by season. The grey polygons in e) and f) give the bounds at 5 mm and 10 mm. (For interpretation of the references to colour in this figure legend, the reader is referred to the web version of this article.)

Table 3
Summary of accuracy of InSAR peat surface motion data from the combined long and short TBN approach. The left and middle columns show the linear multi-annual rates of vertical displacements derived from InSAR and in-situ measurements during the peat camera observation periods for Cors Fochno (C.F.) and Cors Caron (C.C.). The right column shows Pearson's coefficients between the incremental InSAR displacements and the corresponding incremental in-situ displacements. The *p*-values of correlations coefficients are lower than 0.001.

	Peat camera: rate of vertical displacement [mm·yr^{-1}]	InSAR: rate of vertical displacement [mm·yr^{-1}]	InSAR vs in-situ displacement: Pearson's coefficient and RMSE [mm]
C.F. Middle	$-17.96 \pm 0.53(1\sigma)$	$-12.27 \pm 1.20(1\sigma)$	0.86 / 5.57
C.F. Edge	$18.84 \pm 1.32(1\sigma)$	$0.12 \pm 0.07(1\sigma)$	0.92 / 3.81
C.C. West Edge	$2.89 \pm 0.17(1\sigma)$	$-2.97 \pm 0.53(1\sigma)$	0.86 / 2.78
C.C. Northeast Middle	$-2.41 \pm 0.25(1\sigma)$	$-4.66 \pm 0.59(1\sigma)$	0.86 / 2.65
Mean RMSE [mm·yr^{-1}]	**7.08**		**0.88 / 3.70**

peat camera station is excluded.

Statistically, there is no evidence to reject the hypothesis of similarity between InSAR-derived and in-situ displacements (Fig. 11e). Pearson's coefficients are >0.80 for all stations, with an average coefficient at 0.88 (see Table 3). Some 76% of the point deviations are <5 mm, whereas 93% are <10 mm. The distribution of deviations is normal and has the following parameters: μ=1.0 mm; *med*=0.3 mm; σ=5.4 mm, which are characteristic of the distribution for InSAR uncertainty. Conversely, the distributions are not normal in summer and spring, because of most outliers occurring in these periods. In Fig. 11f, the boxplots show that all

deviations are lower than the conventional uncertainties. Figs. S12, S13 and S14 in Supplementary Materials provide additional information on InSAR-derived peat surface displacements.

4.3. InSAR surface displacement versus groundwater level change

There is a close relationship between the short-term (annual) variation in the InSAR-derived surface displacement and the seasonal rise

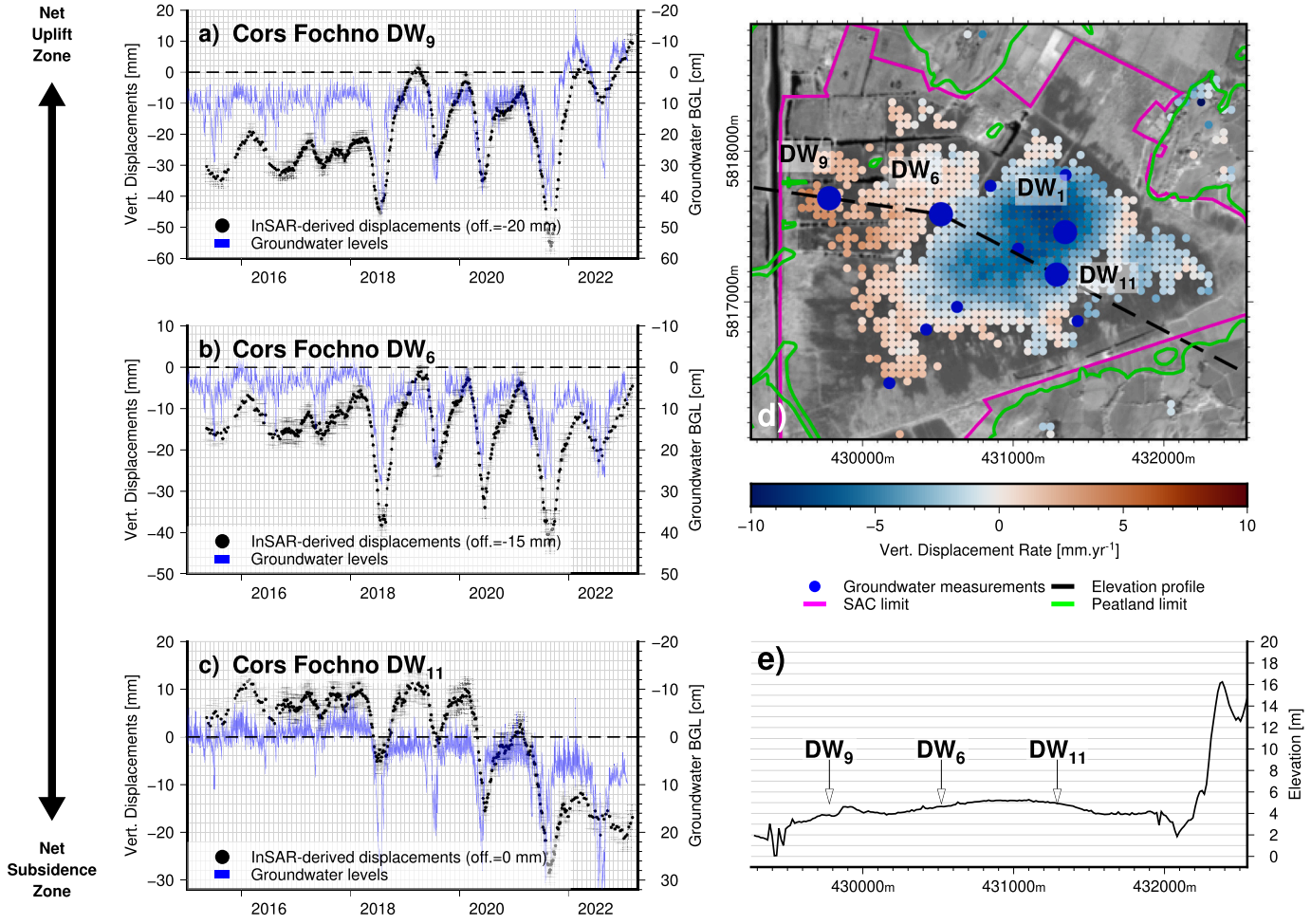

Fig. 12. InSAR-derived vertical displacements and measured groundwater levels. a)-c) Time series of InSAR-derived vertical displacements and groundwater levels for the three selected dip wells on Cors Fochno (BGL: Below ground level). The selected wells are broadly representative of differing long-term trends of peat surface displacement and have complete records for the entire duration of the InSAR observation. Again, the InSAR data represent an average time series for all InSAR points within a 50-m radius of each well site. Note that the values on the vertical axes of each plot differ by a factor of 10 – i.e. InSAR-derived peat surface displacements are approximately ten times less than the groundwater level changes. d) Map of InSAR-derived vertical displacement rates at Cors Fochno with the locations of dip well. e) Lidar elevation (sea level) profile along the selected wells. Basemap Data: near-infrared reflectance image (Band 8) from Sentinel-2 L1C (2018-06-29). Peatland-limit data: see Data availability section.

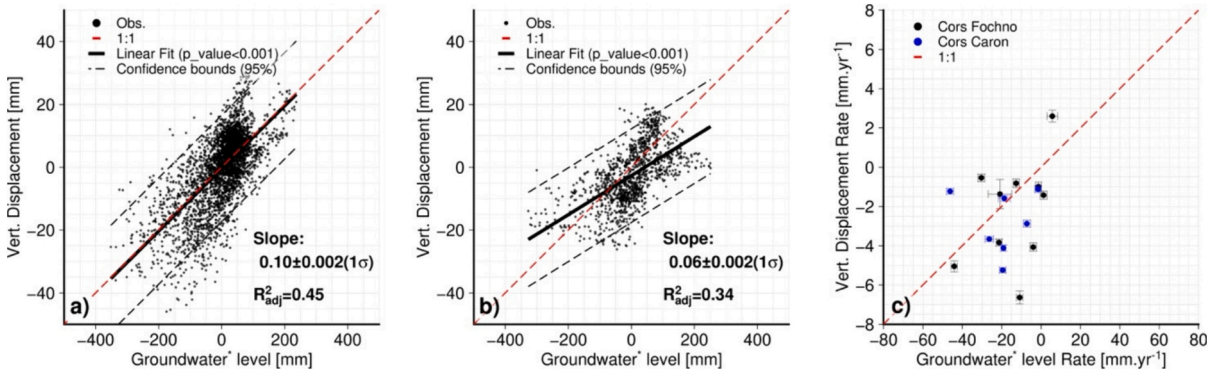

Fig. 13. Cross-plots of InSAR-derived peat surface displacement, groundwater level and long-term rates of change. a-b) Relationship between peat surface displacement and groundwater level changes on Cors Fochno and Cors Caron. *Corrected for peat surface displacements. In b) there is a slight offset of −3 mm between the regression line and the origin, as the time series are not centred exactly at the same period. c) Relationship between long-term rates of groundwater level change and long-term vertical displacement rates at each well. The rates are calculated at each well by simple linear fit to each time series. For Cors Caron, only wells with sufficient groundwater measurements (wells CC_2, CC_3, CC_4, CC_{14}, CC_{15}, CC_{18}, CC_{19}) are presented.

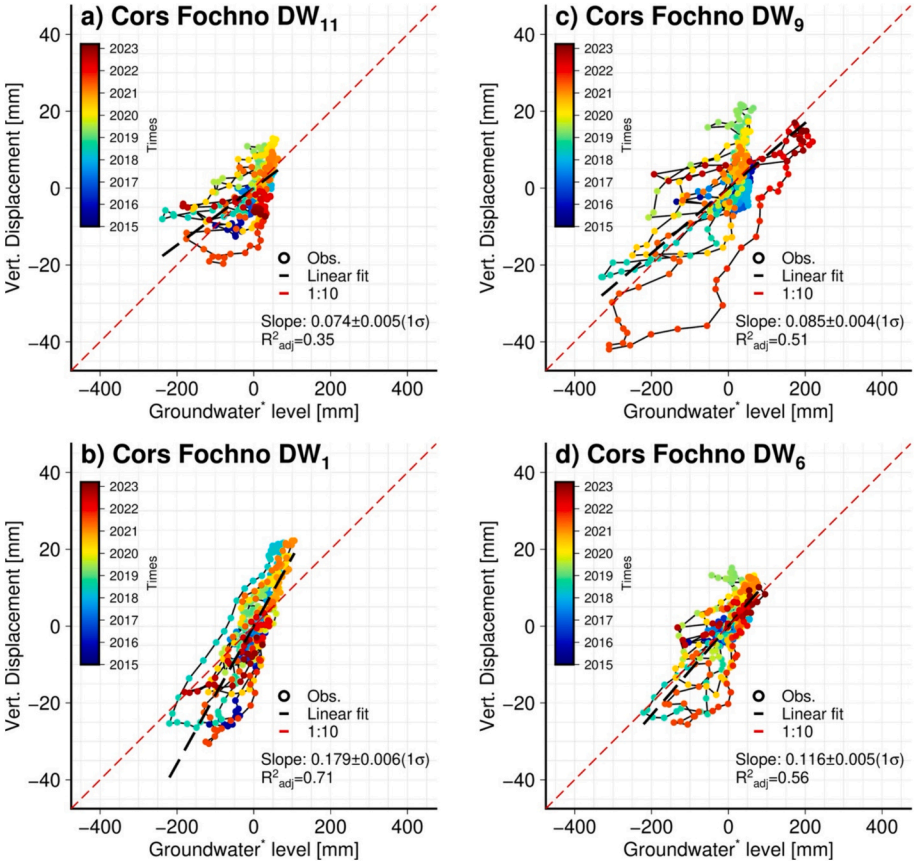

Fig. 14. Cross-plots of InSAR-derived displacements and groundwater levels for four selected individual wells at Cors Fochno. See Fig. 12 for station locations. *Corrected for peat surface displacements and filtered by using a 15-day kernel. All correlations are close to linear with an average ratio of 1:10.

and fall of the groundwater table at Cors Fochno (Fig. 12). Groundwater data for Cors Caron show a similar oscillation, but the time-series are incomplete for most of the InSAR observation period. The complementary figures and full datasets for both bogs are given in Figs. S15, S16 and S17 in Supplementary Materials. In general, the groundwater level changes precede the corresponding motions of the peat surface (see Fig. 12). Moreover, the recovery of the groundwater level to a peak value occurs sooner than the corresponding recovery of the surface level. Thus, the groundwater and bog surface oscillations are slightly out of phase, with the peat surface motion lagging the water table motion by several days/weeks.

For Cors Fochno, the slope of a linear regression between groundwater level change and peat surface displacement – across all wells – is 0.10 ± 0.002 (1σ) (R^2_{ad} = 0.45) (Fig. 13a). For Cors Caron the slope is 0.06 ± 0.002 (1σ) (R^2_{ad} = 0.34) (Fig. 13b). Both correlations are significant at a *p-value* of 0.001. In detail, the individual wells at Cors Fochno show linear regression slopes of between 0.074 ± 0.005 (1σ) and 0.179 ± 0.006 (1σ) (Fig. 14). The amplitudes of groundwater level oscillation therefore relate to those of the InSAR estimated peat surface oscillation with a ratio of roughly 10:1 – i.e., a 10-20 mm change in groundwater level produces a roughly 1–2 mm change in peat surface level.

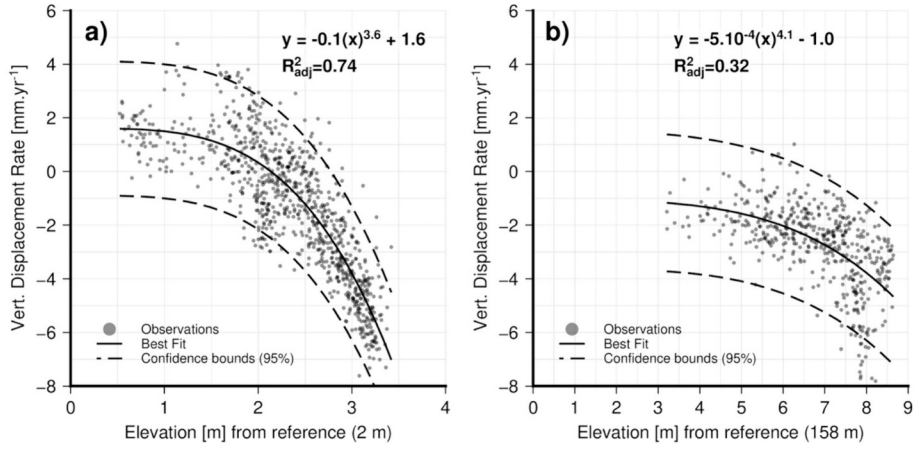

Fig. 15. Relationships between InSAR-derived peat surface displacement and Lidar-derived surface elevation. a) for Cors Fochno. b) for Cors Caron. The elevation references correspond to elevations at peatland edges.

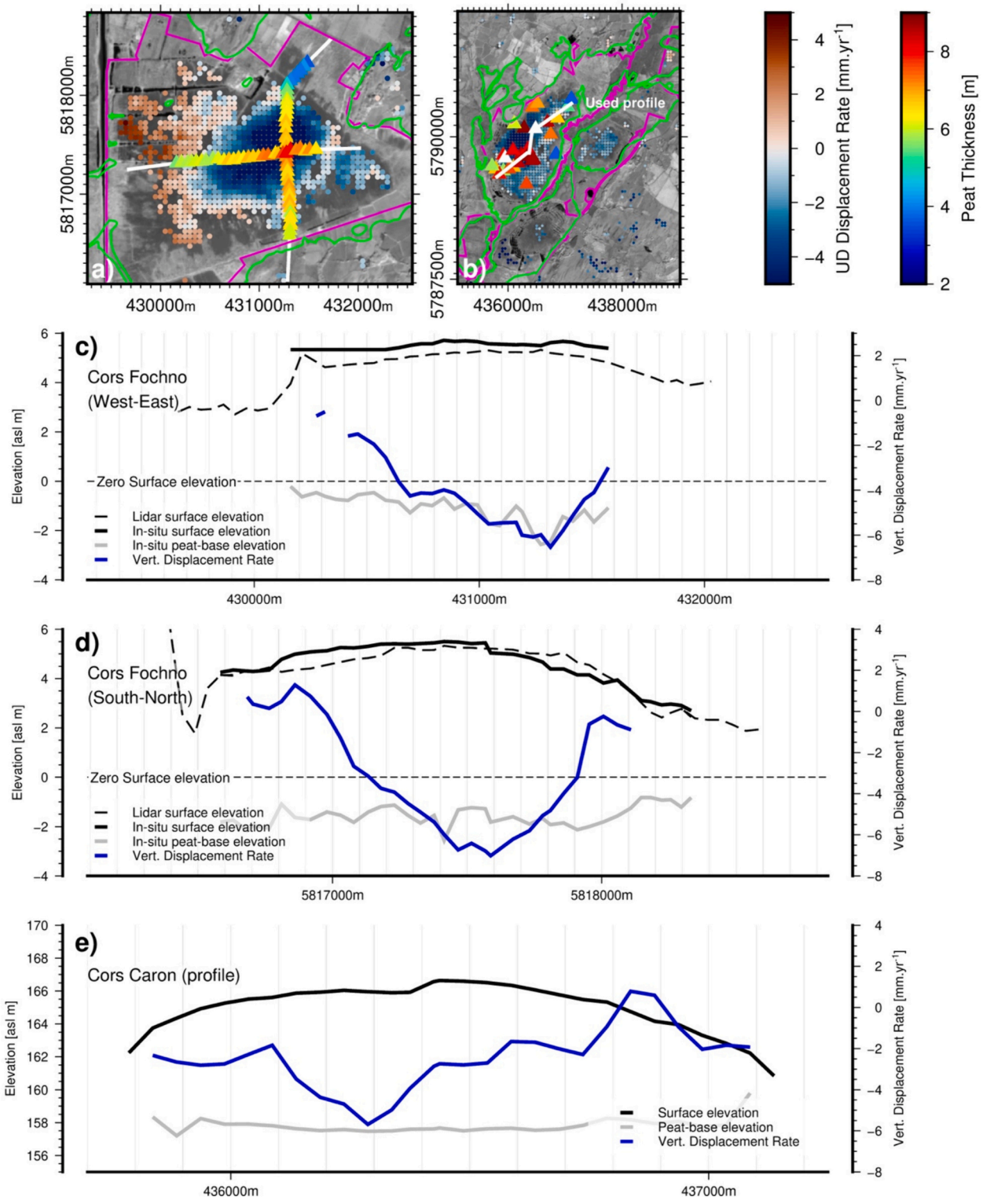

Fig. 16. Peat thickness, surface elevation and InSAR-derived surface motion rates. a) Map of vertical displacement rates with thickness measurements for Cors Fochno represented by triangles. b) Map of vertical displacement rates with thickness measurements for Cors Caron represented by triangles. Both SAC limits are given in magenta. c) West-East cross section on Cors Fochno with vertical displacement rates. d) South-North cross section on Cors Fochno. e) South-west and north-east Cors Caron profile. Peat thickness measurements were linearly interpolated onto the line of profile. The maps are given in UTM Zone 30 N meters Basemap Data: near-infrared reflectance image (Band 8) from Sentinel-2 L1C (2018-06-29). Peatland-limit data: see Data availability section. (For interpretation of the references to colour in this figure legend, the reader is referred to the web version of this article.)

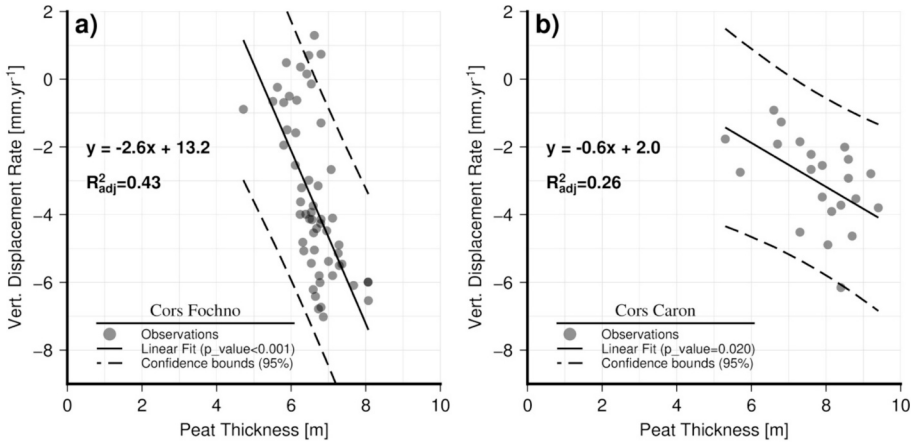

Fig. 17. Relationships between InSAR-derived surface displacement rate and peat thickness. a) for Cors Fochno. b) for Cors Caron.

While at some dip wells there is a correlation between long-term ground surface motion and long-term groundwater level change (Fig. 12), there is not a simple relationship between the long-term linear rate of change of either parameter across all of the wells (Fig. 13c). Localised increases of the winter peaks in groundwater level in the western and southern bog margins by 6–8 cm after summer 2021 (Fig. 12a) coincides with completion of restoration works (bunding) in that area and is reflected in ground surface uplift detected by InSAR.

4.4. InSAR surface displacement versus bog elevation and peat thickness

Surface displacement rates at the two bogs generally increase with peat surface elevation relative to sea level (Fig. 15), such that the greatest and most negative displacement rates are located on the summit of peat domes. For Cors Fochno (Fig. 15a), at first order, a negative 2-order power relationship can be used to predict these two parameters with $R^2_{ad} = 0.74$. For Cors Caron (Fig. 15b), a weaker correlation is observed with $R^2_{ad} = 0.32$.

Displacement rates at the two bogs also generally increase with in-situ peat thickness (Fig. 16), such that the highest displacement rates are located where peat thickness is greatest. This relationship is clearest for the north-south profile through Cors Fochno (see Fig. 16c), less so in the W-E profile (see Fig. 16d). A broadly similar relationship can be seen over Cors Caron (see Fig. 16e). For Cors Fochno (Fig. 17a), at first order, there is a negative linear relationship between these two parameters with a slope of -2.6 ± 0.4 (1σ) mm·yr^{-1}·m^{-1}; $R^2_{ad} = 0.43$; and slope *p-value* < 0.001. For Cors Caron (Fig. 17b), a weaker correlation is observed with a slope of around -0.6 ± 0.3 (1σ) mm·yr^{-1}·m^{-1}; $R^2_{ad} = 0.26$; slope *p-value* $= 0.020$.

5. Discussion

5.1. Ground validation of InSAR displacements from in-situ measurements

The proposed approach of combining results from long and short temporal baseline networks (TBNs) is designed to preserve the long-term (multi-annual) trend of peat surface motion while also mitigating the underestimation of short-term (annual) displacement oscillations (see Fig. 18). From in-situ measurements of displacements at equivalent temporal resolution and precision, based on the newly developed camera-based instruments, our study offers a detailed ground validation that demonstrates the overall success of this method for two temperate raised peatlands.

Ground validation of InSAR-derived surface displacement data has been previously attempted at two temperate oceanic blanket bogs (Marshall et al., 2022) and at a temperate continental raised bog (Tampuu et al., 2023). Marshall et al. (2022) undertook a detailed ground validation of InSAR data from the ISBAS algorithm (Sowter et al., 2013) at two "near-natural" blanket peatland sites in Scotland by using precise levelling of combinations of fixed or floating benchmarks: a 1 km^2 lowland site (6 fixed, 48 floating) and a 1 km^2 upland site (7 fixed, 49 floating). The benchmarks were deployed in 7 clusters per site. The benchmarks were surveyed 16 and 10 times, respectively, over an 18-month observation period in 2017–2019. This method gives a precision of <1 mm and temporal resolution of 1–2 months. Tampuu et al. (2023) undertook a validation of InSAR data from short baseline ("daisy chain") and DS approaches (Tampuu et al., 2022) at a near natural raised bog in Estonia by using a single, automatic, ultrasonic levelling station attached to a metal subsidence pole fixed into the sub-peat mineral soil. The ground level data were recorded over a four-month observation period (July–October) in 2016 with a precision of 3 mm and a temporal resolution of one hour.

For both Marshall et al. (2022) and Tampuu et al. (2023), and indeed for our study, comparison of long-term linear motion rates from InSAR to the in-situ data is not straightforward. This is because of the short duration of the in-situ time-series and the large amplitude of annual oscillations in surface level relative to any linear component in those time series. For Marshall et al. (2022), the average mismatch (RMSE) of their InSAR motion rate to the in-situ motion rate was 16 mm·yr^{-1} for all 14 measurement clusters (without uncertainty consideration); for Tampuu et al. (2023) the mismatch was 29 mm·yr^{-1} for one site; and ours was 7.1 mm·yr^{-1} for four sites. Marshall et al. (2022) noted that most of their ground motion rates from InSAR, although of the same sign as the in-situ rates, consistently underestimated the corresponding rates measured in-situ. We do not see a consistent underestimation by InSAR of the in-situ surface displacement rate, although we have a similar range of mismatch, and we have a smaller number of in-situ stations. Rates from InSAR and in-situ measurements are within uncertainty for two out of four stations (Cors Fochno Middle and Cors Caron East Middle) (Table 3); the others represent in-situ time-series that are either shorter (Cors Fochno Edge) or less complete (Cors Caron West Edge). In this light, the higher RMSE for the results of Marshall et al. (2022) and Tampuu et al. (2023) is possibly to related to the shorter duration of the time-series analysed in those studies. The importance of the length of the time-series for validation of the multi-annual rate can be seen in the reduction of our RMSE to 4.5 mm·yr^{-1} when discounting our shortest in-situ time-series.

On the other hand, we see a much closer agreement between the amplitude of peatland surface oscillation ("bog breathing") measured in-situ and by InSAR. In-situ measurements of surface motion obtained by Marshall et al. (2022) show a range of annual elevation change of 10–60 mm (with one outlier of 120 mm). Tampuu et al. (2022) report an in-situ

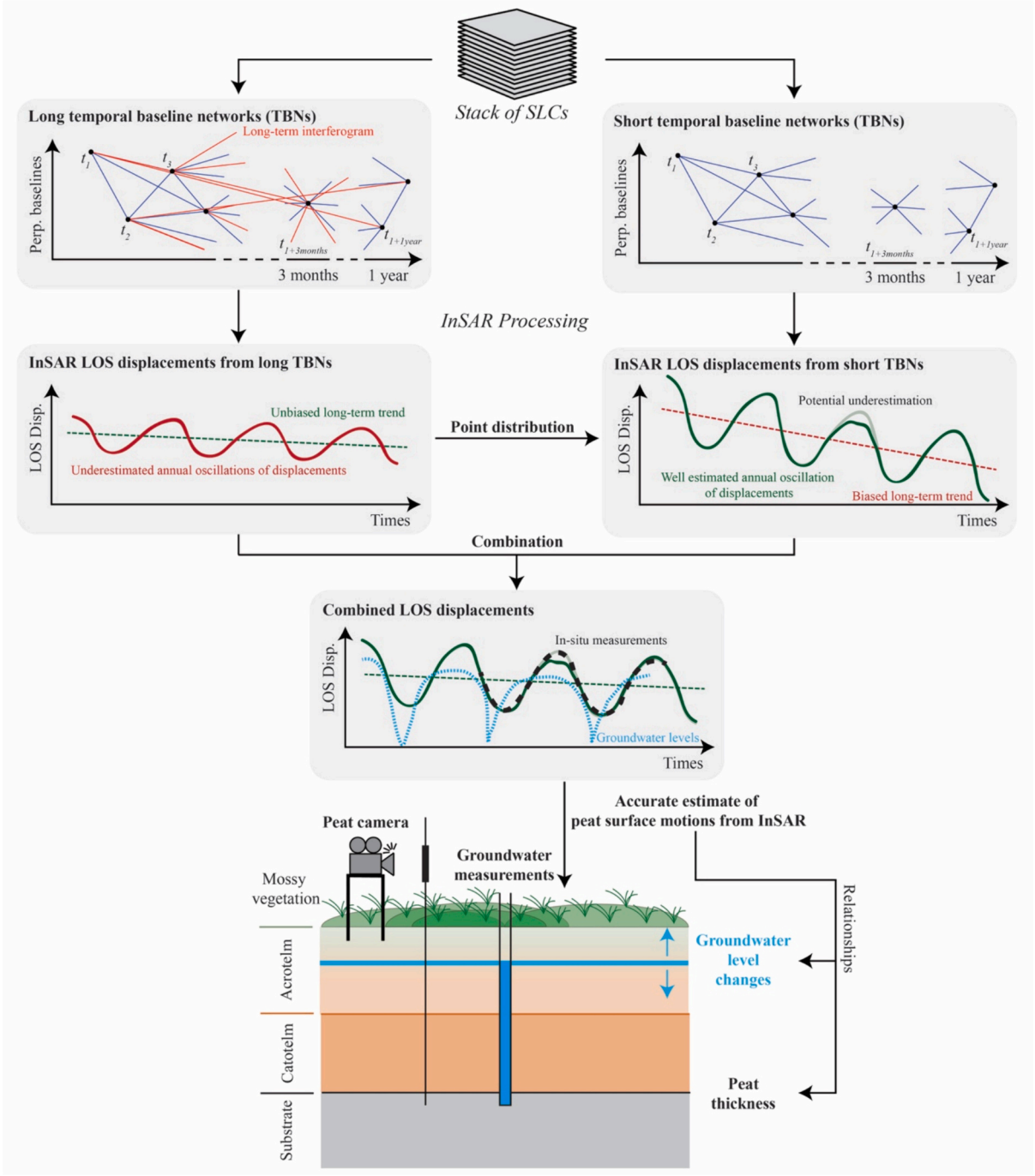

Fig. 18. Summary of the refined InSAR methodology to capture InSAR-derived peat surface displacement on temperate raised bogs and the relationships between remotely sensed and in-situ measurements.

variation of ground level of >50 mm, although for only a four month observation period and thus not a full annual cycle. These ranges are similar to the 10–40 mm range measured at Cors Fochno and Cors Caron. Marshall et al. (2022) observed a maximum decrease of the peat surface elevation in summer of 2018, which is similar to our observations for the summers of 2018–2022. The Pearson's coefficients from the results of Marshall et al. (2022) range from ~0.2 (upland site) to ~0.5 (lowland site). The low and intermediate values of Pearson's coefficient in the Marshall et al. (2022) study are mainly related to underestimation of InSAR-derived displacements during the drought period of 2018. The greater Pearson's coefficient values of 0.8 to 0.9 for Cors Fochno and Cors Caron reflect the fact we achieved a better approximation of the seasonal oscillation of displacement, even in the summer periods, which we attribute to our use of the combined network approach.

It is intriguing that the remotely sensed and in-situ surface displacements correlate so well despite the different spatial scales of observation. InSAR-derived measurements of peatland surface motion represent an aggregate of motion over an area of approximately 2500 m^2, whereas the cameras detect motion over an area of about 1 m^2. Moreover, peatlands are characterised by metre-scale "microtopographic" features (hummocks and hollows) (Graham et al., 2020) that have by differing ecohydrological characteristics (Wu et al., 2011), and are thus suspected to be associated with distinct surface motion behaviours (Marshall et al., 2022). As such, an in-situ measurement that is

strongly anomalous to the main InSAR-defined trend could help to identify instrumental error or more localised micro-topographic effects. We infer that the overall agreement across the varying scales of observation ultimately derives from larger scale controls on peatland surface motions from the groundwater levels and the peat thickness (Fig. 12 to Fig. 17).

In summary, we achieve a robust ground validation of seasonal bog surface oscillation estimated on intact to moderately degraded temperate raised peatlands with InSAR. The validation of long-term surface displacement rates is less robust either because of the large magnitudes of peat surface oscillations relative to the linear component or because of the limited duration of the in-situ time series currently available or because of both these factors. Long-term rates of surface motion at peatlands derived by InSAR or in-situ methods from time-series of less than ~3 years duration should therefore be treated with caution; an analysis of long-term subsidence data from Indonesia excluded all records of less than four years duration for this reason (Evans et al., 2019). On the other hand, the in-situ data show that the seasonal oscillations of peatland surface displacement are well recovered by InSAR, and thus validation of long-term rates from InSAR should be feasible with longer-term time-series of in-situ measurements.

InSAR validation efforts for other geological settings – e.g., volcanoes, urban environments (Ferretti et al., 2007) – typically involve in-situ time-series that are much longer (several years to several decades) and involve ground motions that are of greater magnitude and are more linear (or less oscillatory) in trend than those recorded to date for peatlands. Thus, we anticipate that the mismatch between in-situ and long-term InSAR displacement rates at peatlands will likely be reduced when longer time-series of in-situ displacement data (and more ground stations) are acquired.

5.2. Alterative temporal-baseline networks and unwrapping methods

The long TBN approach proposed by Ansari et al. (2021) is not a unique solution to mitigate the network bias on InSAR displacement rate: another possibility is to use a Delaunay network (De Luca et al., 2022). Delaunay networks have been tested during our computations, but this network type did not have the best results regarding the velocities and annual oscillations of LOS displacements (R = 0.76 and RMSE = 3.94 mm). These results therefore have intermediate precision and accuracy between long and short TBNs (see Figs. S9, S10 and S11 in Supplementary Materials).

Understanding the sources of network-bias is a current challenge (e.g., Ansari et al., 2021; De Zan et al., 2015; Molan et al., 2020; Zheng et al., 2022). In this study, the bias on the multi-annual InSAR displacement rate from the short TBN is less pronounced on Cors Fochno than on Cors Caron (see Fig. 9 and Table 1). Average InSAR coherence for the long TBN interferogram stack is around 0.4–0.5 on the Cors Fochno dome and is 0.3–0.4 on the Cors Caron domes. The degree of displacement rate bias from a short TBN could thus relate to the InSAR coherence on peatlands, although this hypothesis needs further investigation.

The IPTA method uses 3D-unwrapping (i.e., unwrapping in space and in time) to unwrap the interferograms. This method can have limitations when displacements are large on a single interferogram (Werner et al., 2003). Our comparison between 3D-unwrapping and 2D-unwrapping methods undertaken with the short TBNs show that the results are very similar (see Supplementary Figs. S9, S10, S11, S13 and S14), albeit that the 3D-unwrapping method seems slightly more accurate. Pearson's coefficients between in-situ displacements and those from the 2D- and 3D-unwrapping methods range from 0.71 to 0.85, and from 0.76 to 0.91, respectively, with averages of 0.81 and 0.83, respectively. Therefore, our results show that similar ground validation of InSAR-derived displacements can be done if the combined datasets are created from the short TBNs by using 2D unwrapping.

5.3. Possible cause of remaining mismatch in annual oscillations

Although our combined TBN InSAR approach achieves a close match to the seasonal oscillations measured in-situ (Fig. 11 and Table 2), there is still some underestimation of the oscillation amplitudes. These underestimates are most pronounced in the summer periods of relatively dry weather that occurred in the summers of 2019–2021 (Fig. 3), which were associated with sharp drops in the groundwater table (Fig. 12), and so they may relate to changes in soil moisture (Zwieback et al., 2017). Soil moisture changes of peat soils can be large during the summer, but are relatively small during the winter and intermediate seasons (Hrysiewicz et al., 2023). According to the current models of the soil-moisture/InSAR-phase relationships in L-band data, soil moisture changes should cause underestimations of C-band InSAR displacements, decreasing the amplitudes of observed vertical displacements and the InSAR coherence (De Zan and Gomba, 2018; De Zan et al., 2014). This proposition could be tested in future for C-band data by co-location of soil moisture sensors with peat cameras or other instruments for measuring and this isolating the ground motion component.

5.4. InSAR coverage and transferability of the combined TBN method

On Cors Fochno, the InSAR-derived vertical displacement observations cover 51% of the "unmodified" peat dome, 35% of the SAC area and 21% of the wider peat-soil area. On Cors Caron, the respective values are 36%, 19% and 17%. While InSAR points are observed also on some of the "modified bog" land units (see Fig. 2 and Fig. 10), they are almost entirely absent on other land cover or peatland types such as swamp, fen, marsh, grassland and woodland. The principal difference between the raised bog domes and the other landcover types is the nature of the vegetation. The peat domes are dominated by non-vascular (mosses) or low vascular (heather, etc.) vegetation, and they are characterised by relatively small soil moisture changes, so that they represent temporally stable scatterers for C-band InSAR (see Figs. S3 and S4) (Hrysiewicz et al., 2023). In contrast, the other land covers classes are dominated by high vascular vegetation such as reeds, rushes, bushes, and trees that are temporally unstable scatterers, or by low vascular vegetation, such as grass, below which soil moisture can vary considerably (Hrysiewicz et al., 2023; James et al., 2003).

Wider InSAR point coverage can be readily attained with our approach if the quality constraints in the InSAR time-series processing are relaxed. However, this comes with the trade-off that displacement data at the extra points will probably be noisy and inaccurate. Ultimately, the difficulty in attaining reliable C-band InSAR data coverage in the areas outside of the peat domes is related to the poor InSAR coherence (i.e., the poor quality of the InSAR phase) in those areas both in space and in time. Because of the temporal instability in the radar backscattering mechanisms from the vegetation cover in the areas such as fen, marsh and wooded peatland, they are characterised by low to very low InSAR coherence, especially for temporal baselines longer than 12-days (see Figs. S3 and S4 in Supplementary Materials).

In terms of transferability of this method to other peatlands, for example fens, forested peatlands, highly degraded bogs or bare peat, the coherence issue for C-band InSAR remains a major challenge. One potential means to overcome this issue may lie in the future availability, via the proposed NISAR and Tandem-L satellite missions, of open-access L-band data with a similar temporal resolution to Sentinel-1C-band data (~ 12 days). Since the longer L-band radar wavelength enables greater penetration of vegetation, InSAR coherence in L-band should be higher compared to C-band (Umarhadi et al., 2021). A second potential solution may be to augment InSAR processing by using subsets of in-situ data to train an artificial intelligence approaches that can overcome unwrapping issues (Conroy et al., 2024; Conroy et al., 2022). Otherwise, it seems unlikely that any untrained C-band InSAR time series approach will retrieve accurate displacement data in peatland areas of low coherence. Indeed, no ground validation of untrained InSAR data

outside of relatively intact *Sphagnum*-dominated peatland has been presented to date.

5.5. InSAR-derived displacements as a proxy for ecohydrological parameters

Recent works have shown that the annual oscillation of InSAR-derived peat surface displacements relates to the seasonal variation in groundwater levels (Alshammari et al., 2020; Hrysiewicz et al., 2023). In our study, we provide additional links over longer time series and with ground-validation from in-situ displacement measurements. The durations of InSAR time series and groundwater-level measurements allow us to demonstrate that the peat surface motions on the raised bogs lag the water table by several days/weeks. Moreover we achieve a closer approximation of the relationship between the oscillations of groundwater level and the peat surface, with conversion factors of 10:1 for Cors Fochno and 16:1 for Cors Caron (see Fig. 12 and Fig. 13). However, the factor estimated for Cors Caron is less constrained because of the lack of groundwater-level measurements for much of the observation period. Ultimately, if the InSAR displacements can be robustly translated to absolute groundwater levels, they may be used to assist in the estimation of greenhouse gas emissions from peatlands (Evans et al., 2021b; Hoyt et al., 2020).

Lastly, our study provides a first link between the peat thickness, the peat elevation and the long-term displacement rate derived from InSAR. Long-term subsidence rates correlate with both dome elevation, especially on Cors Fochno, and peat thicknesses (see Fig. 17a and Fig. 17b). Such relation has been seen via previous studies using differencing of elevation maps made by in-situ and LiDAR measurements at Clara temperate raised bog, Co. Offaly, Ireland (Regan et al., 2019). These observations could reflect an overriding control on the long-term peat surface motion from compaction of the peat column: i.e., a deeper-seated driving mechanism than that driving the seasonal oscillations. This could provide information on the peat mechanical parameters (density, elastic modulus, etc.). Nevertheless, further studies, with monitoring of deep water levels and more robust estimation of permeability, humification and displacement/thickness relationships, are required to support this interpretation.

6. Summary and conclusions

By using a combination of long and short temporal baseline networks, the InSAR time-series method can be used with Sentinel-1 C-band data to estimate accurately ground surface displacements at relatively intact or moderately degraded temperate raised peatlands (see Fig. 18). This refined InSAR time-series approach is designed to overcome limitations arising from InSAR phase ambiguity and interferogram network bias in the past applications of InSAR for estimating peatland surface motions.

We demonstrate that InSAR estimates of peat surface displacements with this refined approach are valid compared to sub-millimetric in-situ displacement measurements made via peat cameras. In particular, we show that InSAR can capture annual oscillations of the peat surface ("bog breathing") with high accuracy. The multi-annual displacement rates of peat surface motion are not currently validated with the same robustness as the annual oscillations, because of the relatively short in-situ time series and because of the large amplitudes of annual oscillations relative to the rate of linear multi-annual displacement trends.

In-situ data also show that seasonal variations in groundwater levels control the annual oscillation InSAR-derived surface displacement. We observe a lag of several days or weeks between the groundwater level change and the surface level change, and we have shown that the amplitude of groundwater level oscillations are directly related to those of peat surface oscillations with a coarse ratio around 10:1. Longer-term (multi-annual) peat surface subsidence rates at the studies peatland are correlated with dome elevation and peat thickness, which hints at control from long-term compaction and/or consolidation at deeper levels of the peat column. The close agreement between the in-situ measurements of surface displacement on scale of c. 1 m^2 and the surrounding InSAR measurements of surface displacement on a scale of c. 2500 m^2 suggests that the InSAR technique is suitable for upscaling of peatland ecohydrological parameters.

Overall, the refined C-band InSAR method presented here may be used at regional or national scales to monitor the surface displacements of intact to moderately degraded temperate raised bogs. In particular, InSAR-derived displacements could be an accurate proxy of short-term groundwater level changes, which could be a key parameter to validate peatland restoration efforts and to estimate the greenhouse gas emissions. As for any C-band InSAR approach, challenges remain for the wider application and validation of the refined methodology presented here to peatland areas such as fens, swamps, marshes, bare peat and woodland, which are characterised by low InSAR coherence in both space and time. Nonetheless, the refined InSAR method presented here should improve the remote mapping and monitoring of peatland ecohydrological parameters at large scale.

CRediT authorship contribution statement

Alexis Hrysiewicz: Writing – review & editing, Writing – original draft, Visualization, Validation, Methodology, Investigation, Funding acquisition, Formal analysis, Conceptualization. **Jennifer Williamson:** Writing – review & editing, Writing – original draft, Investigation, Formal analysis, Data curation. **Chris D. Evans:** Writing – original draft, Methodology, Conceptualization. **A. Jonay Jovani-Sancho:** Methodology, Investigation. **Nathan Callaghan:** Methodology, Data curation. **Justin Lyons:** Writing – review & editing, Writing – original draft, Investigation, Data curation. **Jake White:** Writing – review & editing, Writing – original draft, Investigation, Data curation. **Joanna Kowalska:** Data curation. **Nina Menichino:** Writing – original draft. **Eoghan P. Holohan:** Writing – review & editing, Writing – original draft, Visualization, Supervision, Project administration, Methodology, Investigation, Funding acquisition, Conceptualization.

Declaration of competing interest

The authors declare that they have no known competing financial interests or personal relationships hat could have appeared to influence the work reported in this paper.

Data availability

The additional figures can be found in the Supplementary Materials. Scripts used to analyse the observations are available from the corresponding author upon reasonable request. The SAC limits, peatland limits and Terrestrial Phase 1 Habitat survey data are available via a UK Open Government Licence (https://www.nationalarchives.gov.uk/doc/open-government-licence/version/3/) from:

- Natural Resources Wales information ©Natural Resources Wales and Database Right. All rights Reserved;
- Ordnance Survey Data (Ordnance Survey Licence number AC0000849444. Crown Copyright and Database Right. ©Crown copyright: Welsh Government;
- and is derived in part from British Geological Survey geology data @ 1:50,000 scale. BGS © UKRI

The HadUK-Grid dataset can be found in Hollis et al. (2019) (UK Open Government Licence, https://www.nationalarchives.gov.uk/doc/open-government-licence/version/3/). Copernicus Sentinel 1 data 2015–2023 are retrieved from ASF DAAC (early 2023), processed by ESA. Copernicus Sentinel 2 data 2016–2023 are retrieved from PEPS CNES (early 2023), processed by ESA. The 2020–2022 Lidar DSM is provided under Open Government Licence (https://www.nationalarchives.gov.uk/doc/open-government-licence/version/3/) by

the Wales government. Peat thickness and water table measurements are available from NRW upon reasonable request.

Acknowledgments

Firstly the authors thank the two reviewers who improved the manuscript via their comments and suggestions and Zhe Zhu, editor-in-chief of RSE. The authors thank past and present members of the iCRAG senior research management team and operations team for their support of the InSAR lab and our related peatland research at UCD. We also thank the staff of GAMMA Remote Sensing AG for training and technical support. We thank NRW staff members Jack Simpson, Rhoswen Leonard, Fleur Miles-Farrier, Ben Soanes, Rebecca Thomas, Osian Fudge, Dan Hersee, & Jon Walker for retrieving the peat height camera data from the field. We acknowledge the European Space Agency (ESA) for the Sentinel-1 and Sentinel-2 data, and NASA for SRTM DEM. We also thank Wessel et al. (2019) and Wessel and Smith (1996) for the development and availability of GMT6 and shoreline database. The authors acknowledge funding from iCRAG, the Science Foundation Ireland Research Centre in Applied Geosciences (iCRAG-Phase 2 – Grand Code: 13/RC/2092_P2) to EPH, and an ESA Living Planet Fellowship to AH (Grand Code: 73738; project name: *Rasied Peatland Ecohydrology Evaluation through Sentinel-1 InSAR data and Machine Learning*). NRW acknowledges funding from the EU LIFE programme for restoration and monitoring work under the "LIFE Welsh Raised Bogs project" (Grant code: LIFE16 NAT/UK/000646).

Appendix A. Supplementary data

Supplementary data to this article can be found online at https://doi.org/10.1016/j.rse.2024.114232.

References

Alshammari, L., Large, D.J., Boyd, D.S., Sowter, A., Anderson, R., Andersen, R., Marsh, S., 2018. Long-term peatland condition assessment via surface motion monitoring using the ISBAS DInSAR technique over the flow country, Scotland. Remote Sens. 10 (7).

Alshammari, L., Boyd, D.S., Sowter, A., Marshall, C., Andersen, R., Gilbert, P., Marsh, S., Large, D.J., 2020. Use of surface motion characteristics determined by InSAR to assess peatland condition. J. Geophys. Res. Biogeosci. 125 (1) https://doi.org/10.1029/2018jg004953.

Amidror, I., 2002. Scattered data interpolation methods for electronic imaging systems: a survey. J. Electron. Imaging 11 (2), 157–176. https://doi.org/10.1117/1.1455013.

Ansari, H., De Zan, F., Parizzi, A., 2021. Study of systematic Bias in measuring surface deformation with SAR interferometry. IEEE Trans. Geosci. Remote Sens. 59 (2), 1285–1301. https://doi.org/10.1109/tgrs.2020.3003421.

Asmuß, T., Bechtold, M., Tiemeyer, B., 2018. Towards monitoring groundwater table depth in peatlands from Sentinel-1 radar data. In: IGARSS 2018–2018 IEEE International Geoscience and Remote Sensing Symposium.

Balenzano, A., Mattia, F., Satalino, G., Pauwels, V., Snoeij, P., 2012. SMOSAR algorithm for soil moisture retrieval using Sentinel-1 data. 2012 IEEE International Geoscience and Remote Sensing Symposium.

Balenzano, A., Mattia, F., Satalino, G., Lovergine, F.P., Palmisano, D., Peng, J., Marzahn, P., Wegmüller, U., Cartus, O., Dąbrowska-Zielińska, K., Musial, J.P., Davidson, M.W.J., Pauwels, V.R.N., Cosh, M.H., McNairn, H., Johnson, J.T., Walker, J.P., Yueh, S.H., Entekhabi, D., Jackson, T.J., 2021. Sentinel-1 soil moisture at 1 km resolution: a validation study. Remote Sens. Environ. 263 https://doi.org/10.1016/j.rse.2021.112554.

Bechtold, M., Schlaffer, S., Tiemeyer, B., De Lannoy, G., 2018. Inferring water table depth dynamics from ENVISAT-ASAR C-band backscatter over a range of peatlands from deeply-drained to natural conditions. Remote Sens. 10 (4) https://doi.org/10.3390/rs10040536.

Biggs, J., Pritchard, M.E., 2017. Global volcano monitoring: what does it mean when volcanoes deform? Elements 13 (1), 17–22. https://doi.org/10.2113/gselements.13.1.17.

Boncori, J.P.M., 2019. Measuring Coseismic deformation with Spaceborne synthetic aperture radar: A review. Front. Earth Sci. 7 https://doi.org/10.3389/feart.2019.00016.

Bradley, A.V., Andersen, R., Marshall, C., Sowter, A., Large, D.J., 2022. Identification of typical ecohydrological behaviours using InSAR allows landscape-scale mapping of peatland condition. Earth Surf. Dyn. 10 (2), 261–277. https://doi.org/10.5194/esurf-10-261-2022.

Bürgmann, R., Rosen, P.A., Fielding, E.J., 2000. Synthetic aperture radar interferometry to measure Earth's surface topography and its deformation. Annu. Rev. Earth Planet. Sci. 28, 169–209. https://doi.org/10.1146/annurev.earth.28.1.169.

Casu, F., Manzo, M., Lanari, R., 2006. A quantitative assessment of the SBAS algorithm performance for surface deformation retrieval from DInSAR data. Remote Sens. Environ. 102 (3–4), 195–210. https://doi.org/10.1016/j.rse.2006.01.023.

Chen, C.W., Zebker, H.A., 2000. Network approaches to two-dimensional phase unwrapping: intractability and two new algorithms. J. Opt. Soc. Am. A Opt. Image Sci. Vis. 17 (3), 401–414. https://doi.org/10.1364/josaa.17.000401.

Chen, C.W., Zebker, H.A., 2001. Two-dimensional phase unwrapping with use of statistical models for cost functions in nonlinear optimization. J. Opt. Soc. Am. A Opt. Image Sci. Vis. 18 (2), 338–351. https://doi.org/10.1364/josaa.18.000338.

Chen, C.W., Zebker, H.A., 2002. Phase unwrapping for large SAR interferograms: statistical segmentation and generalized network models. IEEE Trans. Geosci. Remote Sens. 40 (8), 1709–1719. https://doi.org/10.1109/tgrs.2002.802453.

Connolly, J., Holden, N.M., 2009. Mapping peat soils in Ireland: updating the derived Irish peat map. Ir. Geogr. 42 (3), 343–352. https://doi.org/10.1080/00750770903407989.

Connolly, J., Holden, N.M., 2017. Detecting peatland drains with object based image analysis and Geoeye-1 imagery. Carbon Balance Manag. 12 (1), 7. https://doi.org/10.1186/s13021-017-0075-z.

Conroy, P., van Diepen, S.A.N., Van Asselen, S., Erkens, G., van Leijen, F.J., Hanssen, R. F., 2022. Probabilistic estimation of InSAR displacement phase guided by contextual information and artificial intelligence. IEEE Trans. Geosci. Remote Sens. 60, 1–11. https://doi.org/10.1109/tgrs.2022.3203872.

Conroy, P., Lumban-Gaol, Y., van Diepen, S., van Leijen, F., Hanssen, R., 2024. Monitoring Dutch peatland subsidence using InSAR – First results. In: EGU General Assembly 2024, Vienna, Austria.

De Luca, C., Casu, F., Manunta, M., Onorato, G., Lanari, R., 2022. Comments on "study of systematic Bias in measuring surface deformation with SAR interferometry". IEEE Trans. Geosci. Remote Sens. 60, 1–5. https://doi.org/10.1109/tgrs.2021.3103037.

De Zan, F., Gomba, G., 2018. Vegetation and soil moisture inversion from SAR closure phases: first experiments and results. Remote Sens. Environ. 217, 562–572. https://doi.org/10.1016/j.rse.2018.08.034.

De Zan, F., Parizzi, A., Prats-Iraola, P., Lopez-Dekker, P., 2014. A SAR interferometric model for soil moisture. IEEE Trans. Geosci. Remote Sens. 52 (1), 418–425. https://doi.org/10.1109/tgrs.2013.2241069.

De Zan, F., Zonno, M., Lopez-Dekker, P., 2015. Phase inconsistencies and multiple scattering in SAR interferometry. IEEE Trans. Geosci. Remote Sens. 53 (12), 6608–6616. https://doi.org/10.1109/tgrs.2015.2444431.

Drösler, M., Freibauer, A., Torben, C.R., Friborg, T., 2008. Observations and status of peatland greenhouse gas emissions in Europe. In: The Continental-Scale Greenhouse Gas Balance of Europe. Springer, pp. 243–261. https://doi.org/10.1007/978-0-387-76570-9.

Evans, C.D., Artz, R., Moxley, J., Smyth, E.T., Taylor, E., Archer, N., Burden, A., Williamson, J., Donnelly, D., Thomson, A., Buys, G., Renou-Wilson, F., Potts, J., 2017. Implementation of an Emissions Inventory for UK Peatlands (Updated).

Evans, C.D., Williamson, J.M., Kacaribu, F., Irawan, D., Suardiwerianto, Y., Hidayat, M. F., Laurén, A., Page, S.E., 2019. Rates and spatial variability of peat subsidence in plantation and forest landscapes in Sumatra, Indonesia. Geoderma 338, 410–421. https://doi.org/10.1016/j.geoderma.2018.12.028.

Evans, C.D., Callaghan, N., Jaya, A., Grinham, A., Sjogersten, S., Page, S.E., Harrison, M. E., Kusin, K., Kho, L.K., Ledger, M., Evers, S., Mitchell, Z., Williamson, J., Radbourne, A.D., Jovani-Sancho, A.J., 2021a. A novel low-cost, high-resolution camera system for measuring peat subsidence and water table dynamics. Front. Environ. Sci. 9 https://doi.org/10.3389/fenvs.2021.630752.

Evans, C.D., Peacock, M., Baird, A.J., Artz, R.R.E., Burden, A., Callaghan, N., Chapman, P.J., Cooper, H.M., Coyle, M., Craig, E., Cumming, A., Dixon, S., Gauci, V., Grayson, R.P., Helfter, C., Heppell, C.M., Holden, J., Jones, D.L., Kaduk, J., et al., 2021b. Overriding water table control on managed peatland greenhouse gas emissions. Nature 593 (7860), 548–552. https://doi.org/10.1038/s41586-021-03523-1.

Farr, T.G., Rosen, P.A., Caro, E., Crippen, R., Duren, R., Hensley, S., Kobrick, M., Paller, M., Rodriguez, E., Roth, L., Seal, D., Shaffer, S., Shimada, J., Umland, J., Werner, M., Oskin, M., Burbank, D., Alsdorf, D., 2007. The shuttle radar topography mission. Rev. Geophys. 45 (2) https://doi.org/10.1029/2005rg000183.

Ferretti, A., Prati, C., Rocca, F., 2001. Permanent scatterers in SAR interferometry. IEEE Trans. Geosci. Remote Sens. 39 (1), 8–20. https://doi.org/10.1109/36.898661.

Ferretti, A., Savio, G., Barzaghi, R., Borghi, A., Musazzi, S., Novali, F., Prati, C., Rocca, F., 2007. Submillimeter accuracy of InSAR time series: experimental validation. IEEE Trans. Geosci. Remote Sens. 45 (5), 1142–1153. https://doi.org/10.1109/Tgrs.2007.894440.

Ferretti, A., Fumagalli, A., Novali, F., Prati, C., Rocca, F., Rucci, A., 2011. A new algorithm for processing interferometric data-stacks: SqueeSAR. IEEE Trans. Geosci. Remote Sens. 49 (9), 3460–3470. https://doi.org/10.1109/Tgrs.2011.2124465.

Fiaschi, S., Holohan, E.P., Sheehy, M., Floris, M., 2019. PS-InSAR analysis of Sentinel-1 data for detecting ground motion in temperate oceanic climate zones: A case study in the Republic of Ireland. Remote Sens. 11 (3).

Fritsch, F.N., Carlson, R.E., 1980. Monotone piecewise cubic interpolation. SIAM J. Numer. Anal. 17 (2), 238–246. https://doi.org/10.1137/0717021.

Godwin, H., 1943. Coastal peat beds of the British Isles and North Sea: presidential address to the British Ecological Society 1943. J. Ecol. 31 (2), 199–247. https://doi.org/10.2307/2256548.

Godwin, H., Mitchell, G.F., 1938. Stratigraphy and development of two raised bogs near Tregaron, Cardiganshire. New Phytologist 37 (5), 425–454.

Gorham, E., 1991. Northern peatlands: role in the carbon cycle and probable responses to climatic warming. Ecol. Appl. 1 (2), 182–195. https://doi.org/10.2307/1941811.

Graham, J.D., Glenn, N.F., Spaete, L.P., Hanson, P.J., 2020. Characterizing peatland microtopography using gradient and microform-based approaches. Ecosystems 23 (7), 1464–1480. https://doi.org/10.1007/s10021-020-00481-z.
Habib, W., Ingle, R., Saunders, M., Connolly, J., 2024. Quantifying peatland land use and CO(2) emissions in Irish raised bogs: mapping insights using Sentinel-2 data and Google earth engine. Sci. Rep. 14 (1), 1171. https://doi.org/10.1038/s41598-024-51660-0.
Hanssen, R., 2001. Radar Interferometry: Data Interpretation and Error Analysis, vol. 2. Springer Science & Business Media. https://doi.org/10.1007/0-306-47633-9.
Hiraishi, T., Krug, T., Tanabe, K., Srivastava, N., Baasansuren, J., Fukuda, M., Troxler, T., 2014. 2013 Supplement to the 2006 IPCC Guidelines for National Greenhouse Gas Inventories: Wetlands. IPCC, Switzerland.
Hollis, D., McCarthy, M., Kendon, M., Legg, T., Simpson, I., 2019. HadUK-grid-A new UK dataset of gridded climate observations. Geosci. Data J. 6 (2), 151–159. https://doi.org/10.1002/gdj3.78.
Hooijer, A., Page, S., Canadell, J.G., Silvius, M., Kwadijk, J., Wösten, H., Jauhiainen, J., 2010. Current and future CO2 emissions from drained peatlands in Southeast Asia. Biogeosciences 7 (5), 1505–1514. https://doi.org/10.5194/bg-7-1505-2010.
Hooijer, A., Page, S., Jauhiainen, J., Lee, W.A., Lu, X.X., Idris, A., Anshari, G., 2012. Subsidence and carbon loss in drained tropical peatlands. Biogeosciences 9 (3), 1053–1071. https://doi.org/10.5194/bg-9-1053-2012.
Hooijer, A., Page, S., Navratil, P., Vernimmen, R., Mawdsley, N., 2014. Carbon Emissions from Drained and Degraded Peatland in Indonesia and Emission Factors for Measurement, Reporting and Verification (MRV) of Peatland Greenhouse Gas Emissions. Forda-Mof.Org (May), 50.
Hooper, A., 2008. A multi-temporal InSAR method incorporating both persistent scatterer and small baseline approaches. Geophys. Res. Lett. 35 (16).
Hooper, A., Zebker, H.A., 2007. Phase unwrapping in three dimensions with application to InSAR time series. J. Opt. Soc. Am. A Opt. Image Sci. Vis. 24 (9), 2737–2747. https://doi.org/10.1364/josaa.24.002737.
Hooper, A., Bekaert, D., Spaans, K., Arikan, M., 2012. Recent advances in SAR interferometry time series analysis for measuring crustal deformation. Tectonophysics 514, 1–13. https://doi.org/10.1016/j.tecto.2011.10.013.
Howie, S.A., Hebda, R.J., 2018. Bog surface oscillation (mire breathing): A useful measure in raised bog restoration. Hydrol. Process. 32 (11), 1518–1530. https://doi.org/10.1002/hyp.11622.
Hoyt, A.M., Chaussard, E., Seppalainen, S.S., Harvey, C.F., 2020. Widespread subsidence and carbon emissions across southeast Asian peatlands. Nat. Geosci. 13 (6), 435–+. https://doi.org/10.1038/s41561-020-0575-4.
Hrysiewicz, A., Holohan, E., Donohue, S., Cushnan, H., 2023. SAR and InSAR data linked to soil moisture changes on a temperate raised peatland subjected to a wildfire. Remote Sens. Environ. 291 https://doi.org/10.1016/j.rse.2023.113516.
James, S.E., Pärtel, M., Wilson, S.D., Peltzer, D.A., 2003. Temporal heterogeneity of soil moisture in grassland and Forest. J. Ecol. 91 (2), 234–239. http://www.jstor.org/stable/3599758.
Joosten, H., Sirin, A., Couwenberg, J., Laine, J., Smith, P., Bonn, A., Allott, T., Evans, M., Joosten, H., Stoneman, R., 2016. The role of peatlands in climate regulation. In: Bonn, A., Joosten, H., Evans, M., Stoneman, R., Allott, T. (Eds.), Peatland Restoration and Ecosystem Services. Cambridge University Press, pp. 63–76. https://doi.org/10.1017/cbo9781139177788.005.
Kahaner, D., Moler, C., Nash, S., 1989. Numerical Methods and Software. Prentice-Hall, Inc.
Kim, J.W., Lu, Z., Gutenberg, L., Zhu, Z.L., 2017. Characterizing hydrologic changes of the great dismal swamp using SAR/InSAR. Remote Sens. Environ. 198, 187–202. https://doi.org/10.1016/j.rse.2017.06.009.
Köchy, M., Hiederer, R., Freibauer, A., 2015. Global distribution of soil organic carbon – part 1: masses and frequency distributions of SOC stocks for the tropics, permafrost regions, wetlands, and the world. Soil 1 (1), 351–365. https://doi.org/10.5194/soil-1-351-2015.
Lees, K.J., Quaife, T., Artz, R.R.E., Khomik, M., Clark, J.M., 2018. Potential for using remote sensing to estimate carbon fluxes across northern peatlands - A review. Sci. Total Environ. 615, 857–874. https://doi.org/10.1016/j.scitotenv.2017.09.103.
Leifeld, J., Menichetti, L., 2018. The underappreciated potential of peatlands in global climate change mitigation strategies. Nat. Commun. 9 (1), 1071. https://doi.org/10.1038/s41467-018-03406-6.
Letts, M.G., Roulet, N.T., Comer, N.T., Skarupa, M.R., Verseghy, D.L., 2000. Parametrization of peatland hydraulic properties for the Canadian land surface scheme. Atmosphere-Ocean 38 (1), 141–160. https://doi.org/10.1080/07055900.2000.9649643.
Marshall, C., Sterk, H.P., Gilbert, P.J., Andersen, R., Bradley, A.V., Sowter, A., Marsh, S., Large, D.J., 2022. Multiscale variability and the comparison of ground and satellite radar based measures of peatland surface motion for peatland monitoring. Remote Sens. 14 (2) https://doi.org/10.3390/rs14020336.
Massonnet, D., Feigl, K.L., 1998. Radar interferometry and its application to changes in the earth's surface. Rev. Geophys. 36 (4), 441–500.
Millard, K., Richardson, M., 2018. Quantifying the relative contributions of vegetation and soil moisture conditions to polarimetric C-band SAR response in a temperate peatland. Remote Sens. Environ. 206, 123–138. https://doi.org/10.1016/j.rse.2017.12.011.
Millard, K., Kirby, P., Nandlall, S., Behnamian, A., Banks, S., Pacini, F., 2020. Using growing-season time series coherence for improved peatland mapping: comparing the contributions of Sentinel-1 and RADARSAT-2 coherence in full and partial time series. Remote Sens. 12 (15), 2465. https://doi.org/10.3390/rs12152465.
Minasny, B., Berglund, Ö., Connolly, J., Hedley, C., de Vries, F., Gimona, A., Kempen, B., Kidd, D., Lilja, H., Malone, B., McBratney, A., Roudier, P., O'Rourke, S., Rudiyanto Padarian, J., Poggio, L., ten Caten, A., Thompson, D., Tuve, C., Widyatmanti, W., 2019. Digital mapping of peatlands – A critical review. Earth Sci. Rev. 196 https://doi.org/10.1016/j.earscirev.2019.05.014.
Molan, Y.E., Lu, Z., Kim, J.-W., 2020. Influence of the statistical properties of phase and intensity on closure phase. IEEE Trans. Geosci. Remote Sens. 58 (10), 7346–7354. https://doi.org/10.1109/tgrs.2020.2982062.
Morton, P.A., Heinemeyer, A., 2019. Bog breathing: the extent of peat shrinkage and expansion on blanket bogs in relation to water table, heather management and dominant vegetation and its implications for carbon stock assessments. Wetl. Ecol. Manag. 27 (4), 467–482. https://doi.org/10.1007/s11273-019-09672-5.
Paloscia, S., Pettinato, S., Santi, E., Notarnicola, C., Pasolli, L., Reppucci, A., 2013. Soil moisture mapping using Sentinel-1 images: algorithm and preliminary validation. Remote Sens. Environ. 134, 234–248. https://doi.org/10.1016/j.rse.2013.02.027.
Peng, J., Albergel, C., Balenzano, A., Brocca, L., Cartus, O., Cosh, M.H., Crow, W.T., Dabrowska-Zielinska, K., Dadson, S., Davidson, M.W.J., de Rosnay, P., Dorigo, W., Gruber, A., Hagemann, S., Hirschi, M., Kerr, Y.H., Lovergine, F., Mahecha, M.D., Marzahn, P., et al., 2021. A roadmap for high-resolution satellite soil moisture applications – confronting product characteristics with user requirements. Remote Sens. Environ. 252 https://doi.org/10.1016/j.rse.2020.112162.
Pinel, V., Poland, M.P., Hooper, A., 2014. Volcanology: lessons learned from synthetic aperture radar imagery. J. Volcanol. Geotherm. Res. 289, 81–113. https://doi.org/10.1016/j.jvolgeores.2014.10.010.
Reeve, A.S., Glaser, P.H., Rosenberry, D.O., 2013. Seasonal changes in peatland surface elevation recorded at GPS stations in the red Lake peatlands, northern Minnesota, USA. J. Geophys. Res. Biogeosci. 118 (4), 1616–1626. https://doi.org/10.1002/2013jg002404.
Regan, S., Flynn, R., Gill, L., Naughton, O., Johnston, P., 2019. Impacts of groundwater drainage on peatland subsidence and its ecological implications on an Atlantic raised bog. Water Resour. Res. 55 (7), 6153–6168. https://doi.org/10.1029/2019wr024937.
Renou-Wilson, F., Moser, G., Fallon, D., Farrell, C.A., Müller, C., Wilson, D., 2019. Rewetting degraded peatlands for climate and biodiversity benefits: results from two raised bogs. Ecol. Eng. 127, 547–560. https://doi.org/10.1016/j.ecoleng.2018.02.014.
Sansosti, E., Berardino, P., Bonano, M., Calò, F., Castaldo, R., Casu, F., Manunta, M., Manz, M., Pepe, A., Pepe, S., Solaro, G., Tizzani, P., Zeni, G., Lanari, R., 2014. How second generation SAR systems are impacting the analysis of ground deformation. Int. J. Appl. Earth Obs. Geoinf. 28, 1–11. https://doi.org/10.1016/j.jag.2013.10.007.
Schulz, J., 2004. Late Holocene Mire Development of the Lowland Raised Bogs Cors Caron and Cors Fochno: A Palaeoecological Approach Using High Resolution Macrofossil Analysis University of Southampton.
Smith, P., Bustamante, M., Ahammad, H., Clark, H., Dong, H., Elsiddig, E.A., Haberl, H., Harper, R., House, J., Jafari, M., 2014. Agriculture, forestry and other land use (AFOLU). In: Climate Change 2014: Mitigation of Climate Change. Contribution of Working Group III to the Fifth Assessment Report of the Intergovernmental Panel on Climate Change. Cambridge University Press, pp. 811–922.
Smyth, E.T., Archer, N., Burden, A., Williamson, J., Donnelly, D., Thomson, A., Buys, G., Malcolm, H., Wilson, D., Renou-Wilson, F., 2017. Implementation of an Emissions Inventory for UK Peatlands.
Sowter, A., Bateson, L., Strange, P., Ambrose, K., Syafiudin, M.F., 2013. DInSAR estimation of land motion using intermittent coherence with application to the south Derbyshire and Leicestershire coalfields. Remote Sens. Lett. 4 (10), 979–987. https://doi.org/10.1080/2150704x.2013.823673.
Takada, M., Mishima, Y., Natsume, S., 2009. Estimation of surface soil properties in peatland using ALOS/PALSAR. Landsc. Ecol. Eng. 5 (1), 45–58. https://doi.org/10.1007/s11355-008-0061-4.
Tampuu, T., 2022. Synthetic Aperture Radar Interferometry as a Tool for Monitoring the Dynamics of Peatland Surface. University of Tartu.
Tampuu, T., De Zan, F., Shau, R., Praks, J., Kohv, M., Kull, A., 2022. CAN Bog Breathing be Measured by Synthetic Aperture Radar Interferometry. IGARSS 2022–2022 IEEE International Geoscience and Remote Sensing Symposium.
Tampuu, T., Praks, J., De Zan, F., Kohv, M., Kull, A., 2023. Relationship between ground levelling measurements and radar satellite interferometric estimates of bog breathing in ombrotrophic northern bogs. Mires Peat 29 (17). https://doi.org/10.19189/MaP.2022.OMB.Sc.1999815, 28pp.
Thollard, F., Clesse, D., Doin, M.P., Donadieu, J., Durand, P., Grandin, R., Lasserre, C., Laurent, C., Deschamps-Ostanciaux, E., Pathier, E., Pointal, E., Proy, C., Specht, B., 2021. FLATSIM: the ForM@Ter LArge-scale multi-temporal Sentinel-1 InterferoMetry service. Remote Sens. 13 (18) https://doi.org/10.3390/rs13183734.
Umarhadi, D.A., Avtar, R., Widyatmanti, W., Johnson, B.A., Yunus, A.P., Khedher, K.M., Singh, G., 2021. Use of multifrequency (C-band and L-band) SAR data to monitor peat subsidence based on time-series SBAS InSAR technique. Land Degrad. Dev. 32 (16), 4779–4794. https://doi.org/10.1002/ldr.4061.
Van den Akker, J., Jansen, P., Hendriks, R., Hoving, I., Pleijter, M., 2012. Submerged infiltration to halve subsidence and GHG emissions of agricultural peat soils. In: Proceedings of the 14th International Peat Congress, Stockholm, Sweden.
Wagner, W., Sabel, D., Doubkova, M., Bartsch, A., Pathe, C., 2013. The potential of sentinel-1 for monitoring soil moisture with a high spatial resolution at global scale. Cycle 2009 (November 2009), 18–20.
Wessel, P., Smith, W.H.F., 1996. A global, self-consistent, hierarchical, high-resolution shoreline database. J. Geophys. Res. Solid Earth 101 (B4), 8741–8743. https://doi.org/10.1029/96jb00104.
Wegmüller, U., Werner, C., Strozzi, T., Wiesmann, A., 2004. Multi-temporal interferometric point target analysis. In: Analysis of Multi-Temporal Remote Sensing Images. World Scientific, pp. 136–144.

Wegmüller, U., Werner, C., Strozzi, T., Wiesmann, A., Frey, O., Santoro, M., 2015. Sentinel-1 IWS mode support in the GAMMA software. 2015 IEEE 5th Asia-Pacific Conference on Synthetic Aperture Radar (APSAR).

Werner, C., Wegmuller, U., Strozzi, T., Wiesmann, A., 2003. Interferometric point target analysis for deformation mapping. In: IGARSS 2003. 2003 IEEE International Geoscience and Remote Sensing Symposium. Proceedings (IEEE Cat. No.03CH37477).

Wessel, P., Luis, J.F., Uieda, L., Scharroo, R., Wobbe, F., Smith, W.H.F., Tian, D., 2019. The generic mapping tools version 6. Geochem. Geophys. Geosyst. 20 (11), 5556–5564. https://doi.org/10.1029/2019gc008515.

Wright, T.J., 2004. Toward mapping surface deformation in three dimensions using InSAR. Geophys. Res. Lett. 31 (1) https://doi.org/10.1029/2003gl018827.

Wu, J., Roulet, N.T., Moore, T.R., Lafleur, P., Humphreys, E., 2011. Dealing with microtopography of an ombrotrophic bog for simulating ecosystem-level CO2 exchanges. Ecol. Model. 222 (4), 1038–1047. https://doi.org/10.1016/j.ecolmodel.2010.07.015.

Xu, J., Morris, P.J., Liu, J., Holden, J., 2018. PEATMAP: refining estimates of global peatland distribution based on a meta-analysis. Catena 160, 134–140.

York, D., 1968. Least squares fitting of a straight line with correlated errors. Earth Planet. Sci. Lett. 5, 320–324. https://doi.org/10.1016/s0012-821x(68)80059-7.

Yu, Z., Loisel, J., Brosseau, D.P., Beilman, D.W., Hunt, S.J., 2010. Global peatland dynamics since the last glacial maximum. Geophys. Res. Lett. 37 (13) https://doi.org/10.1029/2010gl043584 n/a-n/a.

Zebker, H.A., Villasenor, J., 1992. Decorrelation in interferometric radar echoes. IEEE Trans. Geosci. Remote Sens. 30 (5), 950–959. https://doi.org/10.1109/36.175330.

Zheng, Y., Fattahi, H., Agram, P., Simons, M., Rosen, P., 2022. On closure phase and systematic Bias in multilooked SAR interferometry. IEEE Trans. Geosci. Remote Sens. 60, 1–11. https://doi.org/10.1109/tgrs.2022.3167648.

Zhou, Z., 2013. The Applications of InSAR Time Series Analysis for Monitoring Long-Term Surface Change in Peatlands University of Glasgow.

Zhou, Z.W., Li, Z.H., Waldron, S., Tanaka, A., 2016. Monitoring peat subsidence and carbon emission in Indonesia peatlands using Insar time series. In: 2016 Ieee International Geoscience and Remote Sensing Symposium (Igarss), pp. 6797–6798. https://doi.org/10.1109/Igarss.2016.7730774.

Zwieback, S., Hensley, S., Hajnsek, I., 2017. Soil moisture estimation using differential radar interferometry: toward separating soil moisture and displacements. IEEE Trans. Geosci. Remote Sens. 55 (9), 5069–5083. https://doi.org/10.1109/tgrs.2017.2702099.